Free turbulent shear layer in a point vortex gas as a problem in nonequilibrium statistical mechanics

Saikishan Suryanarayanan[*] and Roddam Narasimha[†]
Jawaharlal Nehru Centre for Advanced Scientific Research, Jakkur P.O., Bangalore 560064, India

N. D. Hari Dass[‡]
Chennai Mathematical Institute, Kelambakkam 603103, India
and CQIQC, Indian Institute of Science, Bangalore 560012, India

(Received 8 March 2013; revised manuscript received 15 July 2013; published 14 January 2014)

This paper attempts to unravel any relations that may exist between turbulent shear flows and statistical mechanics through a detailed numerical investigation in the simplest case where both can be well defined. The flow considered for the purpose is the two-dimensional (2D) temporal free shear layer with a velocity difference ΔU across it, statistically homogeneous in the streamwise direction (x) and evolving from a plane vortex sheet in the direction normal to it (y) in a periodic-in-x domain $L \times \pm\infty$. Extensive computer simulations of the flow are carried out through appropriate initial-value problems for a "vortex gas" comprising N point vortices of the same strength ($\gamma = L\Delta U/N$) and sign. Such a vortex gas is known to provide weak solutions of the Euler equation. More than ten different initial-condition classes are investigated using simulations involving up to 32 000 vortices, with ensemble averages evaluated over up to 10^3 realizations and integration over $10^4 L/\Delta U$. The temporal evolution of such a system is found to exhibit three distinct regimes. In Regime I the evolution is strongly influenced by the initial condition, sometimes lasting a significant fraction of $L/\Delta U$. Regime III is a long-time domain-dependent evolution towards a statistically stationary state, via "violent" and "slow" relaxations [P.-H. Chavanis, Physica A **391**, 3657 (2012)], over flow time scales of order 10^2 and $10^4 L/\Delta U$, respectively (for $N = 400$). The final state involves a single structure that stochastically samples the domain, possibly constituting a "relative equilibrium." The vortex distribution within the structure follows a nonisotropic truncated form of the Lundgren-Pointin (L-P) equilibrium distribution (with negatively high temperatures; L-P parameter λ close to -1). The central finding is that, in the intermediate Regime II, the spreading rate of the layer is universal over the wide range of cases considered here. The value (in terms of momentum thickness) is 0.0166 ± 0.0002 times ΔU. Regime II, extensively studied in the turbulent shear flow literature as a self-similar "equilibrium" state, is, however, a part of the rapid nonequilibrium evolution of the vortex-gas system, which we term "explosive" as it lasts less than one $L/\Delta U$. Regime II also exhibits significant values of N-independent two-vortex correlations, indicating that current kinetic theories that neglect correlations or consider them as $O(1/N)$ cannot describe this regime. The evolution of the layer thickness in present simulations in Regimes I and II agree with the experimental observations of spatially evolving (3D Navier-Stokes) shear layers. Further, the vorticity-stream-function relations in Regime III are close to those computed in 2D Navier-Stokes temporal shear layers [J. Sommeria, C. Staquet, and R. Robert, J. Fluid Mech. **233**, 661 (1991)]. These findings suggest the dominance of what may be called the Kelvin-Biot-Savart mechanism in determining the growth of the free shear layer through large-scale momentum and vorticity dispersal.

DOI: 10.1103/PhysRevE.89.013009 PACS number(s): 47.27.wj, 47.32.C−, 05.20.−y

I. INTRODUCTION

In a celebrated paper titled Statistical Hydrodynamics, Onsager [1] presented a penetrating discussion of two-dimensional vortex dynamics in a "gas" of positive and negative point vortices in an ideal fluid. (It is convenient to use the word "gas" for describing the problem following Miller [2], in spite of the fact that intervortex interactions described by the Biot-Savart relationship have very long range.) The motion of such a gas is governed by a Hamiltonian and may be expected to lend itself to the formalism of statistical mechanics. (The demonstration that chaotic motion can occur in a collection of more than three vortices [3,4] establishes an underlying stochastic dynamics that justifies a statistical treatment.) Onsager showed that the motion of the vortices could be analyzed in terms of energies and entropies as in classical statistical mechanics, but the temperature derived therefrom would have to be permitted to take negative values. This is because the entropy S as a function of the energy E displays a maximum; hence, $\partial S/\partial E$ can be negative. He also showed that such a gas possesses equilibrium solutions which consist of large-scale vortex clusters or structures, positive and negative segregated from each other.

Since then, considerable work has been done in this direction (see [5], for example). In particular, the nature of the equilibrium state in such a gas has been extensively discussed [6–8], especially in connection with the emergence of large-scale, long-lived vortices in the vortex gas. Several attempts (beginning with Marmanis [9], most recently Chavanis [10]) have also been made to derive a Bogoliubov-Born-Green-Kirkwood-Yvon hierarchy of equations governing vortex distribution functions, based on the Liouville equation, beginning with single-particle analogs of the Boltzmann equation

[*]saikishan.suryanarayanan@gmail.com
[†]roddam@caos.iisc.ernet.in
[‡]dass@cmi.ac.in; dass@cts.iisc.ernet.in

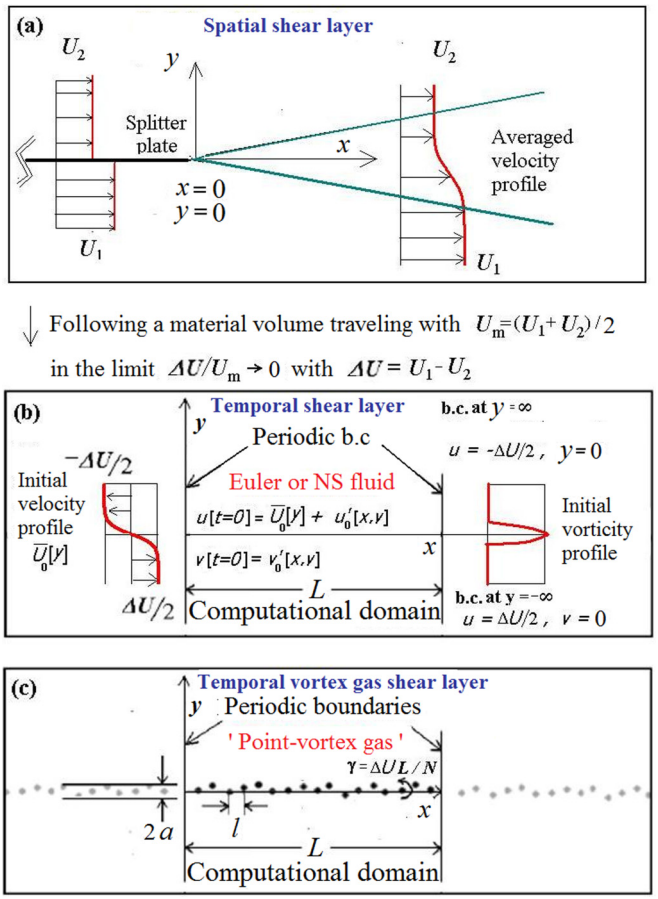

FIG. 1. (Color online) (a) A schematic of a spatially evolving shear layer. (b) The temporal analog (in an Euler or Navier Stokes fluid) often studied in simulations. (Note that we use Reynolds decomposition. $\overline{U}$ indicates averaged velocity that depends only on y, and u' and v' are the x and y components of the fluctuating velocity which has zero mean, respectively. Subscript 0 indicates initial value.) (c) The vortex-gas formulation of the temporal shear layer showing the configuration of vortices at the initial instant. We track the vortices only in the L domain, $0 < x < L$ (which are denoted by dark dots). The governing equations account for the velocities induced by all the vortices in the L domain as well as all those present in $x < 0$, $x > L$ (shown in light colored dots) at separations of $+kL$ and $-kL$, respectively ($k = 1,2,\ldots,\infty$), for each vortex. $l = L/N$ is the initial intervortex separation in x.

and followed by higher members in the hierarchy involving multiple-vortex correlations [11]. A favored target for the application of these ideas has been Jupiter's famous red spot [12,13], seen as one dramatic example of the kind of large-scale long-lived vortex predicted by Onsager.

In the fluid-dynamical literature, observations of large-scale coherent vortical structures have been reported in many turbulent shear flows, including, in particular, the so-called "mixing layer." The spatially developing mixing layer [Fig. 1(a)] is the flow which develops between two streams moving with different velocities U_1 and U_2, separated from each other for $x < 0$ by a thin splitter plate, and mixing with each other for $x > 0$. While extensive measurements have been made on this flow for more than 50 years [14–20], the most striking development has been the convincing demonstration by Brown and Roshko [15] of the until-then unsuspected presence of highly organized large-scale vortices as an integral part of what was a canonical fully developed turbulent flow. This work established that turbulent shear flows could contain ordered motion and led to a search for and the study of such coherent structures in a wide variety of other shear flows [21,22]. The general point that all this work drove home was that the character of turbulent shear flows is fundamentally different from that of statistically homogenous isotropic turbulence, to the extent that ordered motion plays a significant (sometimes dominant) role in determining certain characteristics of sheared turbulence, such as, for example, entrainment of irrotational ambient fluid into rotational turbulent shear flow.

The plane incompressible "temporal" shear layer [Fig. 1(b)] is arguably the simplest conceivable turbulent shear flow, as its specification in the high Reynolds number limit involves only one parameter, namely the velocity differential across the layer. This is a time-dependent flow that is statistically homogeneous in x and evolves temporally in y, from an initial condition at $t = 0$ when the two streams moving at $+\Delta U/2$ and $-\Delta U/2$ are separated by a thin vortical layer at $y = 0$. The temporal shear layer is related via a Galilean transformation to the spatially evolving case in the limit $2(U_1 - U_2)/(U_1 + U_2) \to 0$. Further, it is favored for numerical simulations of the Navier-Stokes equations (e.g., Sommeria *et al.* [23] in two dimensions (2D) and Rogers and Moser [24] in 3D) because of its simplicity and the unambiguous initial and boundary conditions that can be prescribed for the problem. It is usually studied in a domain $0 \leqslant x \leqslant L$ that is periodic in x with period L. This is a valid approximation to the infinite-domain shear layer as long as the relevant length scales in the initial conditions and in the flow field are much smaller than the domain size.

The chief object of the present study is to make a comprehensive simulation of the vortex-gas analog of the temporal shear layer and to carry out a detailed statistical investigation of its evolution. As shown in Fig. 1(c), the problem can be formulated in terms of a row of equally spaced point vortices, located at $t = 0$ along the x axis, say, and allowed to develop in the xy plane for $t > 0$. It is convenient and interesting to study the evolution for a class of initial conditions in which the vortices are given small displacements in y at $t = 0$. This system should not be viewed as a discrete model of a vortex sheet that rolls ups smoothly, but rather as a statistical (chaotic) evolution of a gas of point vortices.

A major argument against the possible relevance of point vortex dynamics to "real-world" (3D Navier-Stokes) turbulent flows is the obvious one about dimensionality. There are, however, real-world flows which are quasi-2D in some sense: The most well known of these is atmospheric motion at higher latitudes, where the large scales are governed by the dynamics of conserved potential vorticity oriented normal to the surface of Earth [25]. Indeed, the reverse energy cascade characteristic of 2D turbulence [26,27] has given much insight into the dynamics of terrestrial and other planetary atmospheres. Another argument is about the complete absence of viscosity (and other molecular transport parameters that may be relevant

for true mixing). No purely inviscid model can handle the phenomena of mixing and dissipation, and consequently both the Richardson cascade and Kolmogorov-type similarity are beyond vortex-gas dynamics. For this reason, we prefer the term "free shear layer" to "mixing layer" in referring to the flow we study.

A related argument [7] is that the long-time evolution of vortex blobs in real fluids cannot be described by vortex-gas motions as the effect of viscosity (say ν), however small, does become manifest on time scales of order ν^{-1}. Interestingly, these arguments take on a different complexion in the free shear layer. Plane 3D Navier-Stokes turbulent shear layers (2D in the mean) do have 3D structures and motions, but the large coherent structures that dominate the growth of the layer (in time or space) are quasi-2D [15,28]. One consequence of such growth is that the local Reynolds number of the flow (based on layer thickness), actually increases linearly with downstream distance x in spatially evolving flow or with time t in the temporally evolving flow. Thus, the effect of viscosity progressively diminishes (equivalently a locally scaled $\nu \to 0$) as $x \to \infty$ or $t \to \infty$, and the viscous time scale of $O(\nu^{-1})$ consequently recedes to ∞ in the limit, *as long as the layer keeps growing*. In any case, the effects of viscosity on vorticity dispersal can, if necessary, be taken into account by the addition of a random walk component in the model [29].

In spite of such objections, early vortex-gas simulations [30,31] were remarkably successful in mimicking several dominant features of evolving shear layers, such as their growth through amalgamation events among the coherent structures. In retrospect, they were limited by inadequate numerical accuracy in integration, small vortex populations, and short integration times. Much more accurate and comprehensive simulations are, however, possible with today's computational resources and, regardless of any possible connection with real shear layers, are of fundamental importance as a study of the simplest conceivable "shear turbulence." They further provide insights into understanding the interplay between chaos and order in such flows through a statistical-mechanics treatment.

Our approach to the problem is akin to that of studying the statistical mechanics of a system of molecules via molecular dynamics. Usual molecular dynamics techniques become ineffective in the presence of long-range forces; but in our context, the two-dimensionality of the problem somewhat compensates for this handicap. We therefore follow the complete evolutionary trajectory of the vortex-gas system all the way from its initial conditions [such as that shown in Fig. 1(c)] to the final asymptotic state (if one exists) as $t \to \infty$. Compared to earlier work, the present simulations are much longer in time (by a factor of 10^4), are far more precise (Hamiltonian conserved to within 0.001% per $L/\Delta U$), and involve large (up to 10^3 member) ensembles; these (as we demonstrate) turn out to be crucial for obtaining the results reported here.

The temporal development of the solution is analyzed from two viewpoints. The first is in terms of statistical mechanics and describes the evolution of the vortex gas, through distribution functions, possible equilibrium states, and temperatures. Such analyses point to the existence of certain universalities that appear to be novel in nonequilibrium statistical mechanics. The second viewpoint is in terms of concepts that have been found useful in the study of turbulent shear flows, such as self-similarity, growth rate of the shear layer, and effect of initial conditions on subsequent flow development. The two viewpoints together yield fresh insights into questions that have been widely discussed but still remain controversial in the fluid-dynamical literature.

The organization of this paper is as follows. In Sec. II, we formulate the problem, present a critical review of earlier calculations, and describe the present computational strategy. Then we discuss the results of our simulations, identifying and describing three distinct regimes in the temporal evolution in Sec. III; detailed results and analyses of the intermediate nonequilibrium universal regime (II) are presented in Secs. IV and V. The domain-influenced regime (III) and the possible final asymptotic state of the system are discussed in Sec. VI. The relevance of the present study to Navier-Stokes shear layers is described in Sec. VII.

II. CURRENT APPROACH

A. Formulation

Many of the earlier vortex-gas studies involve vortices in an infinite plane (e.g., Lundgren and Pointin [6]), in a doubly periodic box (e.g., Montgomery and Joyce [32]) or on a cylinder (e.g., Buhler [33]). The present study of a temporal shear layer in a point vortex gas is formulated as a periodic-in-x array of N point vortices of identical sign and strength ($\gamma = L\Delta U/N$), as shown in Fig. 1(c). Our objective is to study the evolution of this system in (x,y,t) space.

The velocity with which any vortex moves is the vector sum of the velocities induced at its location by all other vortices in the system via the Biot-Savart relationship. In the present setup, the velocity at any vortex (x_i, y_i) in the L domain is the sum of the velocities induced at its location by vortices at $\{x_j + kL, y_j\}, j = 1$ to $N; k = \{-\infty, \ldots, -2, -1, 0, 1, 2, \ldots, \infty\}$. This leads to an infinite convergent series that sums up to the following expressions:

$$\frac{dx_i}{dt} = \sum_{j=1, j\neq i}^{N} \frac{-\gamma}{2L} \frac{\sinh[2\pi(y_i - y_j)/L]}{\cosh[2\pi(y_i - y_j)/L] - \cos[2\pi(x_i - x_j)/L]}, \tag{1}$$

$$\frac{dy_i}{dt} = \sum_{j=1, j\neq i}^{N} \frac{\gamma}{2L} \frac{\sin[2\pi(x_i - x_j)/L]}{\cosh[2\pi(y_i - y_j)/L] - \cos[2\pi(x_i - x_j)/L]}. \tag{2}$$

These equations appear to have been first written down by Friedmann and Poloubarinova [34]. The first reported calculations using (1) and (2) were performed by hand by Rosenhead [35]. Subsequent work using (1) and (2) is reviewed in Sec. II C.

We could consider x an angular variable as the system is x periodic. In the numerical implementation, vortices that leave the domain during the evolution are relocated modulo L using the x periodicity of the system.

The point vortex gas in an infinite plane possesses the Hamiltonian [36]

$$\mathcal{H} = -\frac{\gamma^2}{4\pi}\sum_{i=1}^{N}\sum_{j=1,j\neq i}^{N}\ln[|\mathbf{r}_i - \mathbf{r}_j|/R_0], \tag{3}$$

where $\mathbf{r}_i \equiv (x_i, y_i)$ and R_0 is an arbitrary length scale, often taken as the radius of gyration of the vortex system, $[(1/N)\sum_{i=1}^{N}(x^2+y^2)]^{1/2}$. For the system shown in Fig. 1(c), the Hamiltonian (often also called Kirchhoff's function) takes the form [30]

$$\mathcal{H} = -\frac{\gamma^2}{8\pi}\sum_{i=1}^{N}\sum_{j=1,j\neq i}^{N}\ln\left(\frac{1}{2}\left\{\cosh\left[\frac{2\pi(y_i-y_j)}{L}\right] - \cos\left[\frac{2\pi(x_i-x_j)}{L}\right]\right\}\right). \tag{4}$$

Equations (1) and (2) can be cast in the Hamiltonian form

$$\frac{d(x_i\sqrt{\gamma})}{dt} = \frac{\partial\mathcal{H}}{\partial(y_i\sqrt{\gamma})}; \quad \frac{d(y_i\sqrt{\gamma})}{dt} = -\frac{\partial\mathcal{H}}{\partial(x_i\sqrt{\gamma})}. \tag{5}$$

Thus, the present formulation leads to a Hamiltonian system of $2N$ ODEs that can be solved as an initial-value problem.

B. The major questions

Before posing the major questions, some simple simulations over a relatively long duration are useful. These were performed with $N = 800$, initially equispaced in x and with small initial y values drawn randomly from a uniform probability distribution of amplitude $a(P[y] = 1/(2a)$ for $|y| < a; 0$ for $|y| > a)$.

Figure 2 shows the evolution of vortex positions with time for $a/L = 10^{-6}$. The initial evolution is qualitatively consistent with earlier simulations of this kind [30,31]; in particular, as is clear from Fig. 2, for example, the vortices cluster to form what has been called in the fluid-dynamical literature "coherent structures." These structures grow in size by successive amalgamations among themselves. The average size of the structures and the spacing between them increase with time, while the total number of structures in the domain decreases. We also find that beyond $t\Delta U/L \sim 4$, there is only one structure left in each periodic domain.

To quantify these observations, we introduce a rough measure of layer thickness δ, defined as the maximum y distance at time t between any two vortices in the system (see Fig. 2). (This measure is analogous to the visual thickness of a laboratory mixing layer.) The evolution of δ with time is shown in Fig. 3 for $a/L = 10^{-6}$ and 10^{-2}. (Similar results are obtained if other measures of thickness are used instead of δ.)

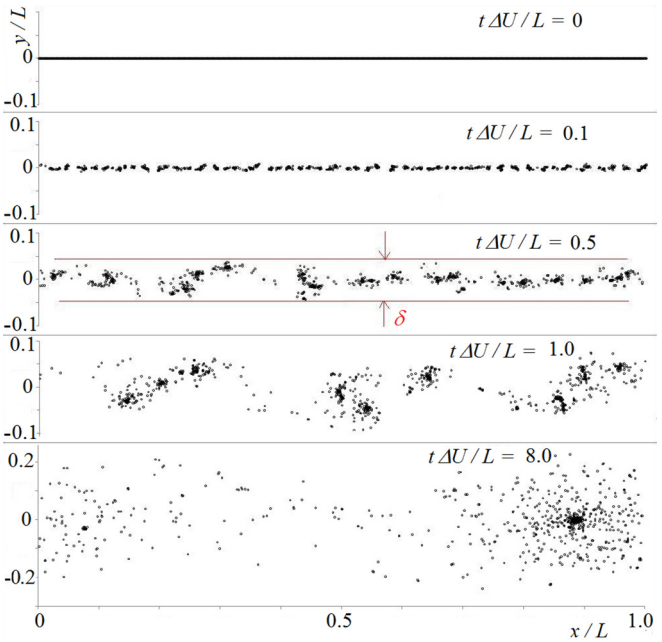

FIG. 2. (Color online) Typical evolution of vortex positions with time ($N = 800, a/L = 10^{-6}$).

It can be seen that for $a/L = 10^{-6}$ δ grows approximately linearly between $0.04 < t\Delta U/L < 2$ but seems to saturate at 0.8 for $t\Delta U/L \geqslant 4$. In the simulation with a much higher initial amplitude of $a/L = 10^{-2}$, the onset of "linear" growth takes place much later at around $t\Delta U/L \sim 0.2$, but the trajectory beyond that point seems to roughly follow the simulation with $a/L = 10^{-6}$, indicating a possibility of universal growth.

These two simulations immediately highlight the presence of at least three regimes in the evolution. For some time after initiation, the solution strongly depends on the initial condition (which we call Regime I), but the effects seem weaker at later times as δ grows linearly in time (Regime II). At longer times (constituting Regime III) the layer thickness seems to fluctuate roughly around a value of $O(1)$. This regime has never been explored in earlier simulations.

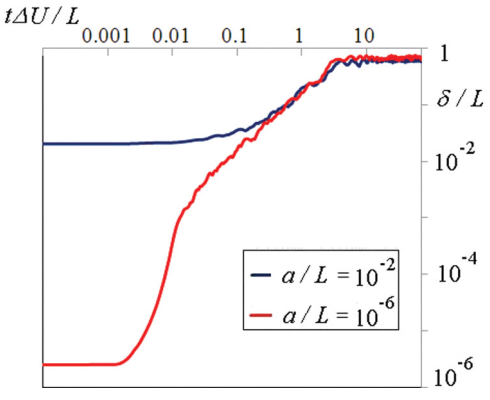

FIG. 3. (Color online) Evolution of thickness δ with time, in exploratory simulations of (1) and (2) (with $N = 800$). Note the existence of different regimes in evolution.

These preliminary simulations raise the following basic questions.

(a) What are the scaling laws in different regimes in the evolution of (1) and (2)?

(b) Are any of the regimes "universal"? If so, which ones and in what variables?

(c) Wherever there is universality, what is the statistical-mechanical explanation?

(d) What is the nature of the solution as $t \to \infty$?

We now briefly review earlier studies of vortex-gas shear layers with the above questions in mind.

C. Review of earlier simulations

Earlier vortex-gas simulations (mostly carried out with a fluid-dynamical perspective) have not explicitly identified the above three regimes and hence no attempt has been made to tackle the questions raised above. This is due to one or more of the following factors.

1. Large statistical uncertainties due to small number of vortices, low accuracy, and non-use of ensemble averaging

The most extensive vortex-gas computations to date are due to Aref and Siggia [31], who have $N = 4096$. They use a cloud-in-cell method which saves computer effort using integer algebra and look-up tables for the calculations, but the technique also introduces a numerical viscosity. With only a single realization they estimated the uncertainty level as 30% in the layer thickness. Delcourt and Brown [30], also using a cloud-in-cell method, reported a 6% change in the Hamiltonian in the computations. No attempt was made to exploit ensemble averaging to arrive at reliable statistics in temporal simulations.

2. Short integration times

The maximum $t\Delta U/L$ reported in earlier work is 1.2 [30]. This is far too short to reach an asymptotic state. For certain classes of initial condition, e.g., those involving long-wave sinusoidal displacements of the point vortices (e.g., Rosenhead [35], Acton [37]), the time of integration is too short even to move out of Regime I.

3. Desingularization and variable number of vortices

Many simulations (most recently [38,39]) adopt desingularization (following Krasny [40]) to study the smooth roll-up of a vortex sheet, as point vortices have been considered to be too chaotic to satisfactorily represent a vortex sheet [41–43] (see also [44,45]). Further, some of these studies adaptively vary the number and hence the strength of vortices to accurately discretize the vortex sheet at all times. However, in the present study, both the flow under consideration and the objectives are different. We wish to study the chaotic evolution of a prototypical turbulent shear flow for which a statistical mechanical treatment is possible. Hence, it is preferable to work with a fixed number of vortices of constant strength, without any desingularization. Some preliminary results [46] suggested that adopting desingularization in the present problem may delay the onset of the linear growth (Regime II) but not the spreading rate. A detailed report on these studies will be presented elsewhere.

D. Present computational strategy

The N point vortices, placed along the x axis with a given intervortex spacing l, are displaced along y by a specified amount at $t = 0$. This displacement is typically randomly generated using a specified probability distribution for each case, but in a few special cases the displacement is taken as a sinusoidal function of x. To obtain the time evolution (1) and (2) are solved numerically using a standard (explicit) fourth order Runge-Kutta algorithm to advance in time the locations of all the vortices. The time step used for integration and the precision of the calculations play an important role in the level of fidelity of the computation to pure Hamiltonian dynamics [47]. (This is also relevant to the issue of recurrence [48], which we discuss in Sec. VI.) To investigate the fidelity of the numerics we perform a set of simulations (with $a/l = 10^{-3}, N = 1600$; detailed results not presented here) with different time steps and precisions. We find that the evolution of the relevant (ensemble-averaged) statistics, such as the layer thickness and single- and two-particle distribution functions, show no significant variation for $\Delta t < 1.0l/\Delta U$, although individual vortex trajectories are found to be different due to the inherently chaotic nature of the system. To understand the role of numerical noise, we simulate cases (with $N = 3200$, not shown here) with $a/l = 0$ and $a/l = 10^{-10}$, each with two different time steps, $\Delta t\Delta U/l = 0.1$ and 0.5 and with double precision. We found that the initial evolution (early Regime I) with $a/l = 0$ was different for the two different values of time step, or (equivalently) of the magnitude of the numerical noise. It has to be noted that this initial condition is a stationary but unstable solution of the point vortex system. Therefore, the numerical noise was essential for triggering the instability and hence its value was important in determining the initial evolution. However, the subsequent evolution, especially Regime II, was independent but for a shift in the virtual origin in time. We find that for $a/l = 10^{-10}$ the evolution did not depend on time step for $t > 0$. This suggests that as long as the "disturbance" in the initial condition is sufficiently large ($a/l \geqslant 10^{-10}$), it dominates the effect of numerical noise throughout the evolution.

The above results suggest the following. There is, of course, nonzero numerical noise in the present study due to the truncation and round-off errors that are inevitable in any computer simulation. Therefore, in principle, we cannot conclude that our simulations are representative of pure Hamiltonian dynamics. However, our results seem to be robustly independent of the magnitude of the numerical noise, provided it is small and nonzero. Most importantly, the spreading rate in Regime II was found to vary by less than a percent as Δt is varied by a factor of 40 (from $0.025l/\Delta U$ to $1.0l/\Delta U$ for a case with $a/l = 10^{-3}, N = 1600$) or between double and quadruple precision simulations (for a case with $N = 400$). Hence, all calculations in this work use double precision and adopt $\Delta t = 0.1l/\Delta U$ as the time step except when stated otherwise. Note that in terms of outer units often quoted in other work, $\Delta t\Delta U/L = 6.25 \times 10^{-5}$ for $N = 1600$ and 7.81×10^{-6} for the simulation with $N = 32\,000$ (we use $\Delta t = 0.25l/\Delta U$ for the latter). This may be compared with the lowest value for $\Delta t\Delta U/L$ of 2×10^{-4} used by Krasny [47]. We also note that the small numerical noise can be

considered a proxy for the nonzero disturbances always found in experiments and may also imply, in part, a correspondingly small numerical viscosity [Reynolds number based on which can be loosely estimated to be $O(10^7)$ based on the decay in the Hamiltonian; details presented elsewhere].

We do not adopt desingularization for the reasons highlighted in Sec. II C. The conservation of the Hamiltonian prevents any two vortices from getting arbitrarily close to each other. We find that using the present algorithm and adopted time step, the distance a vortex moves during any time step rarely exceeds that to its nearest neighbor and is almost always at least an order of magnitude less. Hence, the unbounded velocity in the neighborhood of a point vortex does not present a serious issue in the numerical integration of (1) and (2).

The accuracy of the algorithm has been further assessed in two ways. The first is based on computations on vortices in an infinite plane without the periodicity but otherwise identical initial conditions and parameters as in the shear layer. In this case, the x and y centroids, the second moment, and the Hamiltonian [Eq. (3) are conserved quantities [5]. The Hamiltonian exhibits a deviation of 9×10^{-6} from its initial value at $t\Delta U/L = 0.78$ for $N = 3200$. The first moments of the vorticity distribution about the x and y axes are conserved to within 10^{-16} and 3×10^{-13} times l, and the second moment is conserved to within 1.3×10^{-9} of its initial value. Second, it was found that, in (case R1 of) the present simulations, the variation of the Hamiltonian given by (4) is within 2.5×10^{-5} of the initial value during the time of integration considered (for Regime II, $t\Delta U/L = 0.75, N = 3200$).

Study of Regime III involves long-time integration so a shorter time step of $0.025l/\Delta U$ is adopted. As a result, the Hamiltonian is conserved to within 0.5% for an integration time of $3.6 \times 10^4 L/\Delta U$ (0.58×10^9 time steps). These numbers demonstrate that the current computations are substantially more accurate than any previous work.

Apart from δ (defined in Sec. II B) there are different metrics one can adopt to specify the "thickness" of the layer, such as moments of vortex y positions. In order to enable comparison with Euler and Navier-Stokes shear layers, we generally adopt the so-called momentum thickness θ as the metric, as it is commonly used in the fluid-dynamics literature [20] and in several earlier vortex-gas shear layer studies (e.g., Aref and Siggia [31]). It is defined as

$$\theta[t] = \frac{1}{4}\int_{-\infty}^{\infty} dy \left(1 - \left(\frac{\overline{U}[y,t]}{\Delta U/2}\right)^2\right), \qquad (6)$$

where the x-averaged x velocity defined by

$$\overline{U}[y,t] = (1/L)\int_0^L u[x,y,t]dx$$

is computed by x averaging the induced x velocity u on a grid of 0.4 N points in x and 200 points in y once every 100 time steps. (Note: There are rare occasions when a vortex can come arbitrarily close to a grid point and induce very high velocity. This can reflect in the x-averaged velocities and hence the momentum thickness. In principle, this effect can be addressed by use of a very fine grid and by averaging over a thin strip enclosing the vortex, as this leads to a cancellation of the large induced velocities of opposite signs near the vortex. However, we find that, while computing θ, neglecting the contributions made by those rare instances when x-averaged velocities are not within $\pm U/2$, is an equivalent but easier alternative for numerical implementation. Such a strategy does not change the computed value of θ by more than 1% in 99.9% of cases when $t\Delta U/l > 10$, suggesting that the computed θ is a robust measure.)

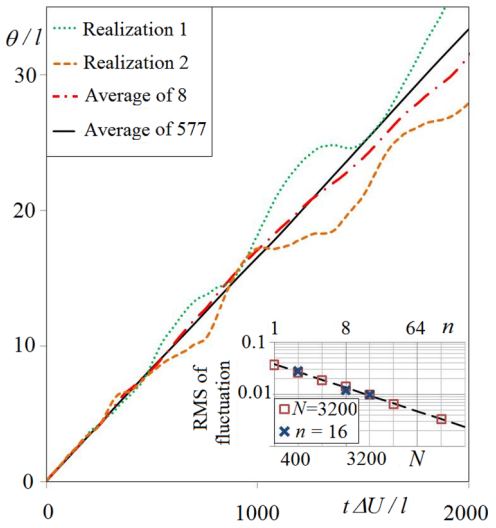

FIG. 4. (Color online) Effect of ensemble averaging. Note that individual realizations have large fluctuations (even for $N = 3200$) and average over a large number of realizations is essential. The rms departure from the respective means (at $t\Delta U/l = 160$) $\sim n^{-1/2}$ (shown in dashed line) for a given N and $\sim N^{-1/2}$ for a given n.

E. Ensemble averaging

In computational statistical-mechanics ensemble averaging is commonly adopted to reduce statistical fluctuations. For measurements in statistically stationary turbulent flow in fluid dynamics long-time averaging is often adopted as an alternative to ensemble averaging. As the present system is nonstationary in time but statistically homogeneous in x, x averaging is, in principle, equivalent to ensemble averaging. However, we find that an average over an ensemble of realizations (with initial conditions varied within a clearly specified class) is worthwhile due to the following reasons.

We first note that the statistical error (at a given $t\Delta U/l$) may be expected to vary with N as $N^{-1/2}$ (observed also in our present simulations, as shown in Fig. 4), while the computational effort grows as N^2. If we simulate n realizations with N vortices each, the error goes as $(nN)^{-1/2}$ while the computational effort goes as nN^2, i.e., as n^{-1} for a given error. It is this result that makes the ensemble approach so attractive. However, a sufficiently large $N = L/l$ is required in each realization to have a sufficiently long extent and preserve the inherent distinction between the different regimes observed in Fig. 3. But, once N is sufficiently large, the ensemble averaging approach is computationally far more economical. It also has the practical advantage of using parallel computers more effectively, as different "realizations" can be independently simulated on different processors without any need for data communication.

We also find that the ensemble average of θ computed from the x-averaged velocity profile for each realization is not very different (for large N and n) from the value computed from the ensemble average of the (x-averaged) velocity. Throughout this study, we use the former for the sake of numerical convenience. We also note that, for a given initial-condition class, the standard deviation of the Hamiltonian across realizations is never more than 1% of its mean value for present simulations with more than 400 vortices and is often much less: e.g., less than 0.01% for the set of simulations presented in Sec. IV. Hence, the present ensemble can be considered a microcanonical ensemble.

We discuss the significant implications of inadequate averaging in detail in Sec. VII.

III. RESULTS: THE THREE REGIMES IN EVOLUTION

With the objective of determining the precise scaling laws in each of the three regimes already noted in the simulations, we carry out several additional simulations with different initial displacements drawn from uniform random distributions with amplitudes ranging from $10^{-4}l$ to $10l$, with different domain sizes ranging from $200l$ to $1600l$, and with averages over up to 12 realizations. A summary of the results is presented in Fig. 5 as a composite diagram. In order to shed light on the different scaling laws in the different regimes, it is useful to adopt, depending on the regime, either δ or θ as the measure of the layer thickness and $l/\Delta U$ or $L/\Delta U$ as the time scale. It is therefore important to pay attention to the precise variables used as the abscissa and ordinate in Fig. 5.

Initial-condition dominated Regime I. As shown in Fig. 5, the evolution is widely different for different initial conditions during the initial Regime I. Here δ is adopted as the measure of layer thickness as θ cannot be accurately determined for $t\Delta U/l < 10$ (see Sec. II D). It is seen that the duration of this regime (t_{RI}), varying from 10^{-2} to 10 times $l/\Delta U$ for the cases considered here, strongly depends on the initial conditions, as shown in an inset in Fig. 5. For certain initial-condition classes, including those where the y displacement of vortices is a long-wave sinusoidal function of x, Regime I may be much longer [$O(10^3)l/\Delta U$ for case P1 shown in Sec. IV]. In such cases the transition to Regime II may even be nonmonotonic.

Domain-limited Regime III. Jumping now to Regime III, we find from Fig. 5 that, at times comparable to or larger than the domain size time scale (i.e., $t\Delta U/L > 1$), the effects of finite domain size become noticeable and the growth of the layer departs from the linear variation with time seen in Regime II. As shown in the inset in Fig. 5, the dynamics in the initial stages of Regime III are governed by the interactions among a small number of coherent structures. Figure 5 shows the approximate collapse of θ/L vs $t\Delta U/L$ beyond $t\Delta U/L = 1$ for data obtained from simulations with L/l ranging from 200 to 1600, confirming that the scaling length changes from l in Regime I (and II) to L in Regime III (and also II; see below). Beyond $t\Delta U/L \sim 4$ the magnitude of changes in

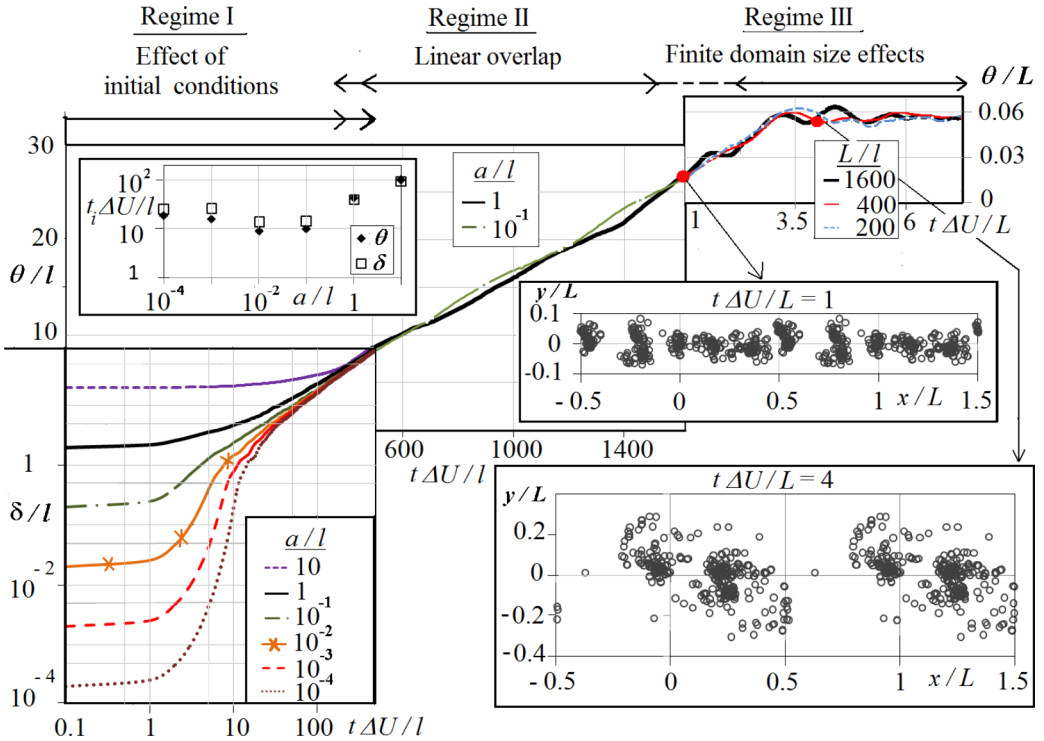

FIG. 5. (Color online) Composite diagram showing effect of initial conditions and domain size on the evolution of the shear layer. Note the use of δ and θ in different parts of the diagram and the change in the abscissa from $t\Delta U/l$ with a logarithmic scale up to 500, the linear scale between 500 and 1500, and a switch to $t\Delta U/L$ thereafter. Appropriate changes have been made on both the abscissa and the ordinate to ensure that the evolution curve should go smoothly from one regime to the next. The inset on the top left gives the variation of initial transient with the amplitude of the initial vortex displacement. The two insets on the right give pictures of the configuration of the vortices at $t\Delta U/L = 1$ (upper) and at $t\Delta U/L = 4$ (lower).

the thickness of the layer (in a statistical sense) is greatly reduced. This is because there is only one structure left in the domain (see lower inset in Fig. 5), and hence there is no further opportunity for the layer to grow by amalgamation among structures. The evolution of the single structure to its final stage and its connections to vortex-gas equilibrium are discussed in Sec. VI.

The intermediate linear Regime II. It can be observed from Fig. 5 that between Regimes I and III is an intermediate Regime II in which the layer exhibits linear growth.

From a mechanics viewpoint, the transition between the short-time initial and long-time asymptotic states is governed by an intermediate asymptotics that can be derived by methods similar to those used by Millikan [49] in channel flow and Kolmogorov [50] in turbulence spectra (see Narasimha [51]).

The evolution of a measure of thickness $\hat{\delta}[t]$ can be written as

$$\frac{d\hat{\delta}}{d(t\Delta U)} = F_i\left[\frac{t\Delta U}{l}, \frac{L}{l}, \frac{\{x_i[0], y_i[0]\}}{l}\right]. \tag{7}$$

Note that one can equivalently use any characteristic length scale of the initial condition instead of l.

If we hypothesize that the solution (7) evolves to a state independent of the precise initial configuration for sufficiently large $t\Delta U/l$, the third argument of F_i in Eq. (7) will drop out in the limit. In what may be called the long-time or "outer" limit (see Van Dyke [52]), $t\Delta U/L = O(1)$, the solution may be expected to be dominated by the finite domain size and scale as

$$\frac{d\hat{\delta}}{d(t\Delta U)} = F_o\left[\frac{t\Delta U}{L}\right], \quad t\Delta U/l \to \infty, \quad t\Delta U/L \text{ fixed}. \tag{8}$$

Note that the above argument would strictly hold only in the early part of Regime III ($t\Delta U/L < 4$), as we show in Sec. VI.

If we postulate an overlap between (7) and (8) in the simultaneous limits $t\Delta U/l \to \infty$ and $t\Delta U/L \to 0$ (in the spirit of matched asymptotic expansions [52]), the only possibility is an overlap Regime II in which

$$\frac{d\hat{\delta}}{d(t\Delta U)} = C_1, \tag{9}$$

where C_1 is independent of time; i.e., the layer thickness grows linearly with time.

IV. UNIVERSALITY AND FLUID-DYNAMICAL EQUILIBRIUM OF REGIME II

Is C_1 universal (for different initial-condition classes)? In order to answer this question, a total of 11 cases, with widely different initial-condition classes for y_{i0}, domain length, number of vortices, and ensemble size have been performed. The results are presented in Fig. 6.

The initial conditions considered (details in Table I) include uniform random distributions (cases R1, R2, R3, R4-32000, R4-1600, R4-400) with amplitude ratio a/l varying from 10^{-8} to 10^{-1}, Gaussian distributions(G1), bimodal distributions in the form of sums of symmetric or asymmetric displaced Gaussians (respectively BM1, BM2), and distributions varying

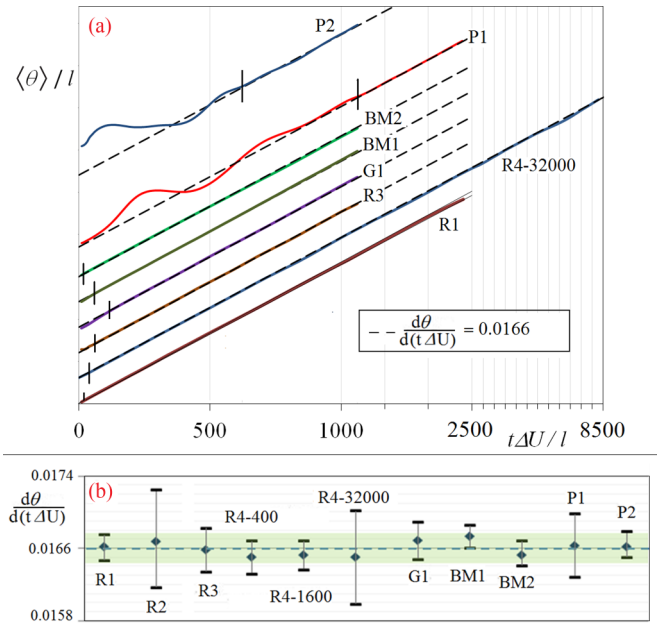

FIG. 6. (Color online) (a) Universality of Regime II. Note the wide range of initial conditions including those with very long transients. See the change in scale beyond $t\Delta U/l$ of 1000. (b) Estimate of uncertainties in Regime II growth rate. The error bars show the 95% confidence limits (computed using Student's t distribution). The dotted line is drawn through the reference (R1) growth rate.

sinusoidally in x (P1 and P2). In the case of random initial conditions each realization is initialized with a different set of random numbers from the same class. The different "realizations" required for ensemble averaging for sinusoidal initial conditions ($y_{oi} = a_w \sin[2\pi x_i/\Lambda + \phi_0]$, where a_w and Λ are the amplitude and wavelength of the perturbation) can be generated with different initial phases (ϕ_0) of the wave at $t = 0$ with respect to that at the beginning of the domain ($x = 0$). (Small differences in numerics lead to different solutions in terms of individual vortex trajectories over time due to the chaotic nature of the system, but not in the statistics.) This strategy is used in case P2. An alternative is to add a small random disturbance to the wave at the initial instant and draw it from some specified distribution. This is done for case P1, whose discussion is deferred to Sec. VII.

The respective growth histories in Regime II are shown in Fig. 6. A best fit to the growth is obtained by minimizing $\sum_{t=t_{\rm IIb}}^{t=t_{\rm IIe}} (1 - ((At\Delta U + B)/\theta[t]))^2$ with respect to A and B, where $t_{\rm IIb}$ and $t_{\rm IIe}$ are the estimated beginning and end of Regime II. We choose $t_{\rm IIe}$ to be $0.8t\Delta U/L$ or the end of the simulation, whichever is earlier. The locations of $t_{\rm IIb}$ are indicated in Fig. 6 by short vertical bars. We take as reference the best-fit value for R1 ($N = 3200; n = 577$) in which Regime II extends over more than two decades in $t\Delta U/l$ (20–2400) and $d\theta/dt = 0.0166\Delta U + \text{const}$.

Figure 6(b) shows the ensemble-averaged best-fit growth rates and the 95% confidence limits for the eleven cases considered. Based on these results, the evolution of momentum thickness in Regime II is given by

$$\theta_{\text{Regime II}} = 0.0166(\pm 0.000\,15)t\Delta U + C_3, \tag{10}$$

TABLE I. Details of different cases and the respective spreading rate in Regime II.

Code	N	n	Initial conditions	Best fit $\frac{d\theta}{d(t\Delta U)}$
R1	3200	577	Uniform random $a/l = 5 \times 10^{-2}$	0.016 618
R4	**400**	512	Uniform random $a/l = 1 \times 10^{-3}$	0.016 51
R4	1600	512	Uniform random $a/l = 1 \times 10^{-3}$	0.016 532
R4	**32 000**	14	Uniform random $a/l = 1 \times 10^{-3}$	0.016 506
R2	10 000	11	Uniform random $a/l = 1 \times 10^{-1}$	0.016 685
R3	1600	256	Uniform random $\mathbf{a/l = 1 \times 10^{-8}}$	0.016 587
G1	1600	512	Gaussian $\sigma/\mathbf{l = 1}$	0.016 689
BM1	1600	1024	Bimodal $\sigma_1/l = 1 \times 10^{-1}$ $\sigma_2/l = 1 \times 10^{-1}$ $d/l = 6 \times 10^{-1}$	0.016 737
BM2	1600	1024	Bimodal $\sigma_1/l = 1 \times 10^{-2}$ $\sigma_2/l = 2 \times 10^{-2}$ $d/l = 4 \times 10^{-2}$	0.016 534
P1	3200	288	Sinusoidal $a_w/l = 4 \times 10^{-1}$ $a_n/l = 4 \times 10^{-4}$ $\lambda/l = 100$	0.016 635
P2	1600	512	Sinusoidal $a_w/l = 1.188 \times 10^{-2}$ $a_n/l = 0$ $\lambda/l = 50$	0.016 624

with a universal slope. The generally nonuniversal intercept ranges from $-3.1l$ (P2) to $0.7l$ (G1) in the present simulations (the corresponding "virtual origin", i.e., the intercept to the Regime II growth line on the time axis would be $186l/\Delta U$ and $-42l/\Delta U$). The departures in Regime II growth rate across the wide range of initial conditions are within a band of $\pm 1\%$ from the reference value, and may be compared with the 30% uncertainty reported by Aref and Siggia [31]. Figure 7 shows snapshot of vortex positions in Regime II for R4-32000.

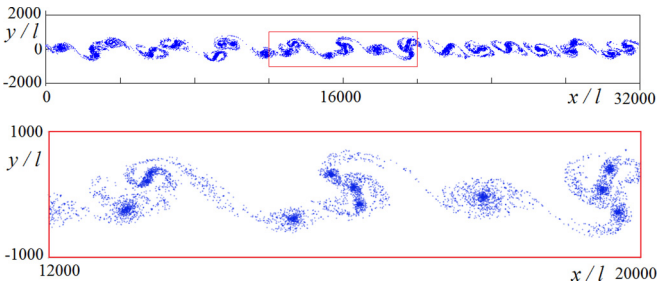

FIG. 7. (Color online) Snapshot of vortex positions at the end of the simulation ($t\Delta U/L = 0.25$) of one realization of R4-32000. Note that there are around 2000 vortices per structure, and the vortices resolve features within each structure as well as in the "braids."

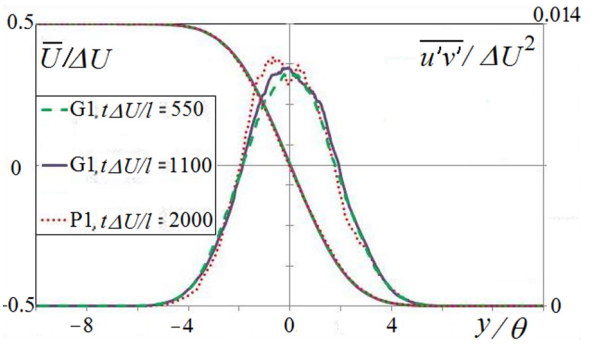

FIG. 8. (Color online) Self-similarity and universality of x-averaged (fluid) velocity and "Reynolds shear stress" profiles. The latter has been evaluated using integral of vorticity flux (computed from 64 member ensembles).

Figure 8 shows that profiles of mean velocity and Reynolds shear stress for the case P1 and (at two different times) for the case G1. (It is easily shown from the Reynolds-averaged Euler equations that, for the 2D temporal mixing layer considered, the streamwise momentum balance reduces to $\partial\tau/\partial y = -\overline{v'\omega'}$, where $\tau = \overline{u'v'}$ is the Reynolds shear stress and $\overline{v'\omega'}$ is the mean vorticity flux at y. In the present vortex-gas shear layer, the Reynolds shear stress at y can be computed by evaluating $-\sum v_i\gamma_i/L$ over all the vortices with $y_i < y$, where v_i is the vertical velocity induced on the ith vortex.) In the normalization used in similarity theory [53], with velocities scaled with ΔU and normal displacement with θ, it is seen that the three profiles agree for both mean velocity and Reynolds stress, indicating both self-similarity and universality, and hence of (fluid-dynamical) equilibrium in the sense of Narasimha and Prabhu [54]. This implies that universality extends to any measure of thickness based on the mean velocity profile.

For two illustrative cases (G1 and P2), Fig. 9 shows that the moments of the vortex positions, $m_k = \langle |y_i|^k \rangle^{1/k}$, become universal multiples of the momentum thickness at sufficiently long times, in general longer for the sinusoidal initial condition (P2) compared to the Gaussian initial condition (G1), establishing similarity and universality irrespective of the measure used to describe layer thickness.

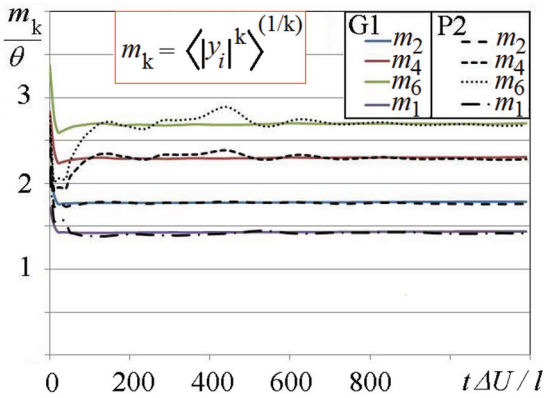

FIG. 9. (Color online) Evolution of various measures of thickness based on vortex positions for G1 and P2. All of them settle to a constant factor of θ in Regime II for the two very different initial conditions.

V. THE NONEQUILIBRIUM STATISTICAL MECHANICS OF REGIME II

Is there a statistical-mechanical explanation for the observed universality in Regime II? To answer this, we first explore the possibility of describing Regime II using approaches based on existing "vortex-gas kinetic theories" inspired by the Boltzmann equation [9–11,13,55,56]. This may be done by computing the single- and two-vortex distribution functions in the present simulations. We consider cases R4-1600 and R4-400 as they involve a short Regime I and large ensemble sizes and also provide an opportunity to assess the effect of the number of vortices on the simulations. We also analyze simulations with $a/l = 2, N = 400$ to study the effect of initial conditions (if any). The domain is divided into 40×40 boxes of equal size, the width of each box (Δx) being fixed, while the height (Δy) increases linearly with time to cover the entire layer with optimum resolution at each instant. The number of vortices present in each box at a given time is averaged over an ensemble of 512 realizations. This gives the single vortex distribution function $f_1[x,y,t]$, which is normalized such that $\sum f_1 \Delta x \Delta y = L^2$. (We use this normalization for convenience as it renders f_1 dimensionless, in contrast with the conventional definition.) Note that this single-particle distribution function is related to the ensemble-averaged vorticity as $f_1 = \langle\omega\rangle/(\Delta U/L)$. Since the system is homogeneous in x, large-ensemble averages should be independent of x. However, even for the ensemble sizes used in the present simulations, there are fluctuations in f_1 of up to 10% along x. Therefore, in order to improve the statistics, $f_1[x,y,t]$ is averaged over x to obtain $\overline{f_1}[y,t]$, with $\sum \overline{f_1} \Delta y = L$.

From Fig. 10(a), which shows Regime II data at different times for two cases in which initial conditions and number of vortices are both different, $\overline{f_1}[y,t]$ takes the universal form given by

$$\frac{\theta[t]}{L}\overline{f_1}[y,t] = \Phi_1\left[\frac{y}{\theta[t]}\right], \tag{11}$$

where Φ_1 is the self-similarity function; i.e., the function $\overline{f}_1[y,t]$ of two independent arguments is reduced to a function a single argument $y/\theta[t]$.

Further, when $t\Delta U$ is such that $C_3 \ll t\Delta U \ll L$, Eq. (10) shows that θ is linear in $t\Delta U$. Therefore, in the limit of $t/t_{\mathrm{RI}} \to \infty$ (equivalently, $L/l \to \infty$ for a given a/l), $\overline{f_1}$ follows self-similar scaling in Regime II:

$$\overline{f_1}[y,t] = \frac{L}{t\Delta U}\Phi_2\left[\frac{y}{t\Delta U}\right]. \tag{12}$$

This relation is closely followed for the case R4-1600 beyond $t\Delta U/L = 0.2$, as seen in Fig. 10(b). This result is important, for the similarity form of the solution (12) is not admitted by the kinetic theory proposed by Chavanis (Eq. 129 of [55]).

To explore this issue further, we compute the two-vortex distribution function $f_2[x_1,y_1,x_2,y_2]$ by ensemble averaging the product of the number of vortices in two given boxes around (x_1,y_1), (x_2,y_2) at a given time. We define the two-vortex correlation function f_2' as

$$f_2'[x_1,y_1,x_2,y_2] = f_2[x_1,y_1,x_2,y_2] - f_1[x_1,y_1]f_1[x_2,y_2]. \tag{13}$$

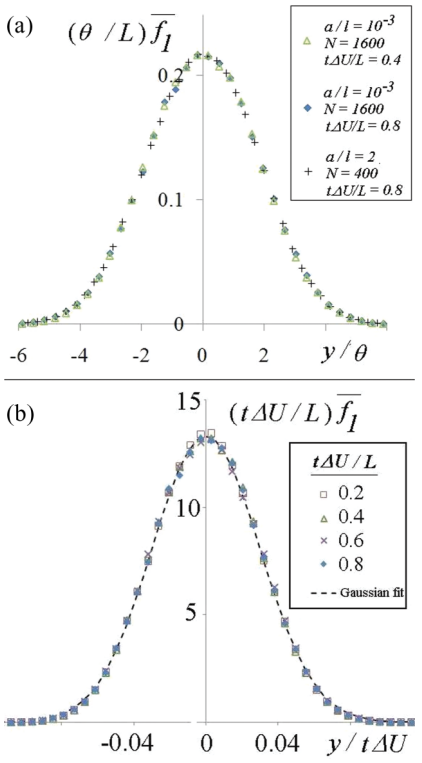

FIG. 10. (Color online) (a) Single-particle distribution function for different cases when scaled by momentum thickness. (b) Self-similar scaling of single-particle distribution function (for R4-1600).

If $f_1[x_1,y_1]$ is statistically independent of $f_1[x_2,y_2]$, i.e., if we make the analog of Boltzmann's "molecular" chaos assumption, then the right hand side will vanish. Now due to x homogeneity f_2' should depend only on y_1,y_2 and $|x_1 - x_2|$ for a sufficiently large ensemble. Again, averaging over x to improve the statistics we present $\overline{f_2'}[|x_1 - x_2|,y_1,y_2]$ versus $|x_1 - x_2|$ for fixed y_1 and y_2 (both set close to zero) in Fig. 11. It can be immediately seen that f_2' shows a systematic variation with $|x_1 - x_2|$ and can take values several times that of the local $f_1 * f_1$ at small $|x_1 - x_2|$. Furthermore, f_2' takes both large

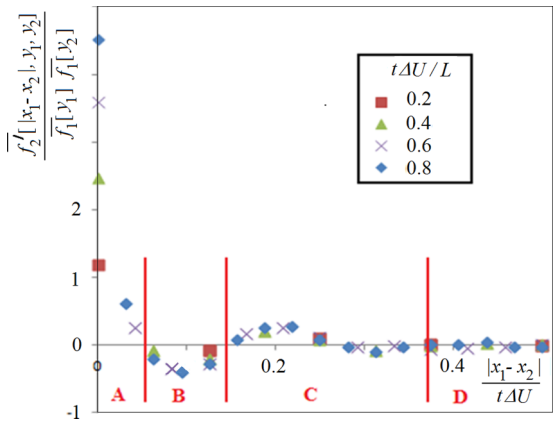

FIG. 11. (Color online) Temporal evolution of f_2' as a function of x separation at $y_1 = y_2 = 0.0029t\Delta U$ during Regime II of case R4-1600. Note that there is self-similar scaling except at very small $|x_1 - x_2|$.

positive and large negative values, indicating the presence of strong two-vortex correlations of both signs alternating between each other.

To understand the $|x_1 - x_2|$ dependence of f_2' exhibited in Fig. 11, it is instructive to relate it to the coherent structures in the flow, in particular to the length scales associated with their size and the spacing. These are obtained as follows. From an analysis of the snapshots of the vortex configurations such as those in Fig. 7, we find that the average number of coherent structures in the L domain during Regime II is approximately $4L/t\Delta U$ in the limit $C_3 \ll t\Delta U \ll L$, and hence the average x distance between their centers is approximately $(1/4)t\Delta U$, equivalently about 15θ from Eq. (12). Further, from Fig. 7, the size of the structures is approximately half the spacing between their centers, i.e., about $(1/8)t\Delta U$ or 7.5θ. The nearest "braid" region therefore lies between approximately 0.06 and $0.19t\Delta U$ from the center of a structure.

Returning to Fig. 11, it is seen that the functional dependence of $\overline{f_2'}$ on the x separation exhibits four distinct regions.

(A) At small separations ($|x_1 - x_2| < 0.05t\Delta U$ near the x axis), which approximately corresponds to distances within the same structure (i.e., less than half the average size of the structure), $\overline{f_2'}$ is several times $\overline{f_1} * \overline{f_1}$ and positive.

(B) At distances $0.05t\Delta U < |x_1 - x_2| < 0.15t\Delta U$, $\overline{f_2'}$ is of order $\overline{f_1} * \overline{f_1}$ and negative. This clearly characterizes the braid region between two neighboring structures.

(C) At somewhat larger separations $\overline{f_2'}$ oscillates between positive and negative values, with amplitude diminishing with distance. The first positive peak is located at approximately $0.22t\Delta U$, which is roughly the distance to the center of the next structure, and reflects the degree of order in the arrangement of nearby structures. The peaks progressively decay with larger separation.

(D) At large distances ($|x_1 - x_2| \geqslant 0.4t\Delta U$) $\overline{f_2'}$ is negligible, indicating that vortex positions are uncorrelated. It is only in this region that the analog of Boltzmann's "molecular chaos" is valid.

It can be seen from Fig. 12 that the observed values of $\overline{f_2'}$ are N independent to a very good approximation. Hence, in the vortex-gas shear layer, f_2' can neither be neglected as in most Boltzmann-inspired "kinetic theories" [10,13,55,56] nor be considered as $O(1/N)$ as proposed in some recent work [11]. This indicates that large values of f_2' in the present system are not finite-N effects, but rather an indication of the strong correlations attributable to the observed size and spacing of the coherent structures.

Further, it can also be seen from Fig. 12 that $\overline{f_2'}$ at two different values of y coordinates is qualitatively similar but quantitatively different. This may be related to the scatter of y locations of the coherent structures, but a detailed analysis of the complete structure of f_2' will be separately presented.

Also shown in the same figure is the variation of f_2' for two initial conditions whose amplitudes differ by three orders of magnitude. The differences in f_2' are negligible, in general, but become barely noticeable between the two cases as $|x_1 - x_2| \to 0$. On returning to Fig. 11, we can also observe the lack of self-similarity of f_2' as $|x_1 - x_2| \to 0$. However, there does not seem to be any evidence against self-similarity and universality of f_1 (Fig. 10).

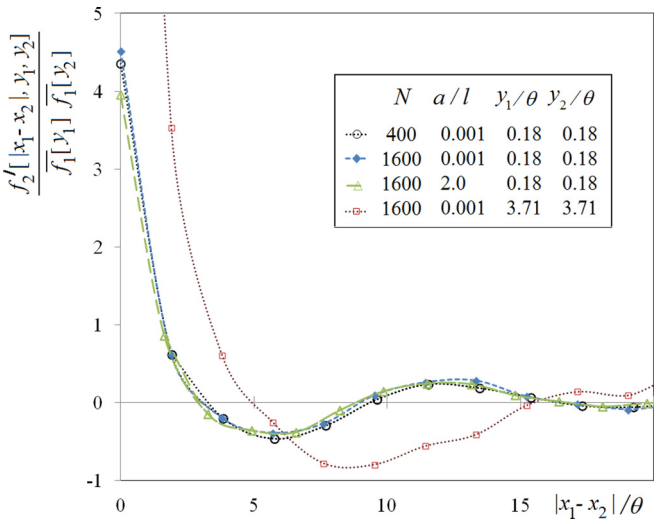

FIG. 12. (Color online) Variation of $\overline{f_2'}$ with number of vortices (note that the maximum value of f_2 changes by less than 5% from $N = 400$ to 1600, which is within the statistical uncertainty), initial conditions and with y/θ at $t\Delta U/L = 0.8$.

A possible heuristic explanation for this apparent inconsistency is as follows. When the structures grow in size with time, the average intervortex spacing is expected to increase in most parts of the system. In order to conserve the Hamiltonian, this has to be balanced by reduction of intervortex spacing somewhere else in the system, possibly near the center of the structures. This explanation would not be inconsistent with the observation self-similarity of f_2' except at the center of the structures, i.e., when $|x_1 - x_2| \to 0$, where the normalized f_2' increases with time (i.e., the relative vortex density, and hence the correlations, increase at the center of the structures as they grow in size with time). Similarly, different classes of initial conditions would have different values for the Hamiltonian, whose conservation would demand a variation in density of cores and hence correlations across the different initial-condition classes. We return to this in Sec. VI.

However, it has to be noted that the coherent structures occur at different y locations, as observed in Figs. 2 and 7. As a consequence, on averaging over different realizations, the effect of the vortex distribution within the clusters plays an insignificant role in determining the single-particle distribution function f_1. This is also explained in detail during the analysis of Regime III in the following section. We show that as long as more than one structure is present (which is also the case in Regime II), the vortex distribution within the structure does not significantly alter either the single-particle distribution function and hence the mean vorticity and velocity profiles, or the layer thickness, but becomes important when only one structure is left in the domain.

The central message these analyses convey is that the vortex-gas shear layer is strongly correlated and existing "kinetic theory" approaches based on the Boltzmann equation that neglect correlations or consider them as $O(1/N)$ are inapplicable in Regime II. Furthermore, several of the features of the two-particle correlation function can be qualitatively explained or interpreted in terms of the observed properties of the coherent structures.

VI. REGIME III AND CONNECTIONS TO STATISTICAL-MECHANICAL EQUILIBRIUM

Most statistical-mechanical analyses of a system involve questions regarding its final or asymptotic state. For an isolated vortex-gas system, it was proposed by Onsager that for energies greater than a critical value, the formally defined temperature becomes negative and leads to the emergence of large-scale order by clumping of like-signed vortices. These ideas were further developed by Joyce and Montgomery [57] and by Lundgren and Pointin [6]. The latter derived a closed-form expression for the equilibrium single-particle distribution of point vortices of same sign and identical strength in an infinite plane. Miller [2] and Robert and Sommeria [58] developed statistical theories for the Euler equation (which is a fluid-dynamic analog of the Lynden-Bell theory [59] of stellar systems). The kinetic theory of vortices formulated by Chavanis [10,55], in a spirit similar to that of the Boltzmann equation for gases, considers the evolution of the system as a relaxation to a "Boltzmann distribution" defined for the vortex gas.

The present simulations provide a basis for an assessment of the various theoretical ideas concerning relaxation to an asymptotic state. Figure 13 shows the evolution of momentum thickness during long-time vortex-gas simulations in six cases. We recall from Sec. III that Regime III is that part of the solution where the statistics depart from the universal linear growth of Regime II and exhibit a dependence on (and scale with) domain size. Figure 13 reveals that this regime has three distinct subregimes. It can be observed in all the cases simulated here that, immediately following Regime II, there is a rapid but nonlinear and domain-dependent increase in thickness that scales with L and extends to about $t\Delta U/L \sim 4$. We call this Regime III(a). Beyond this, the thickness evolves very slowly over very long time scales, changing over $10^4 L/\Delta U$ by less than 20% of its value at $4L/\Delta U$. This subregime is labeled III(b) and appears to reach asymptotically a final state of constant thickness, Regime III(c).

Each of these subregimes of Regime III is now considered in turn.

Regime III(a). From Fig. 13(a), it is seen that although the evolution of momentum thickness begins to depart from the linear growth of Regime II at around $(t - t_0)\Delta U/L \sim 1$, it remains universal (with L as the length scale) and is independent of initial conditions or N, until about $t\Delta U/L \sim 3$. We find that in Regime III(a) the number of structures can vary from 4 to 1.

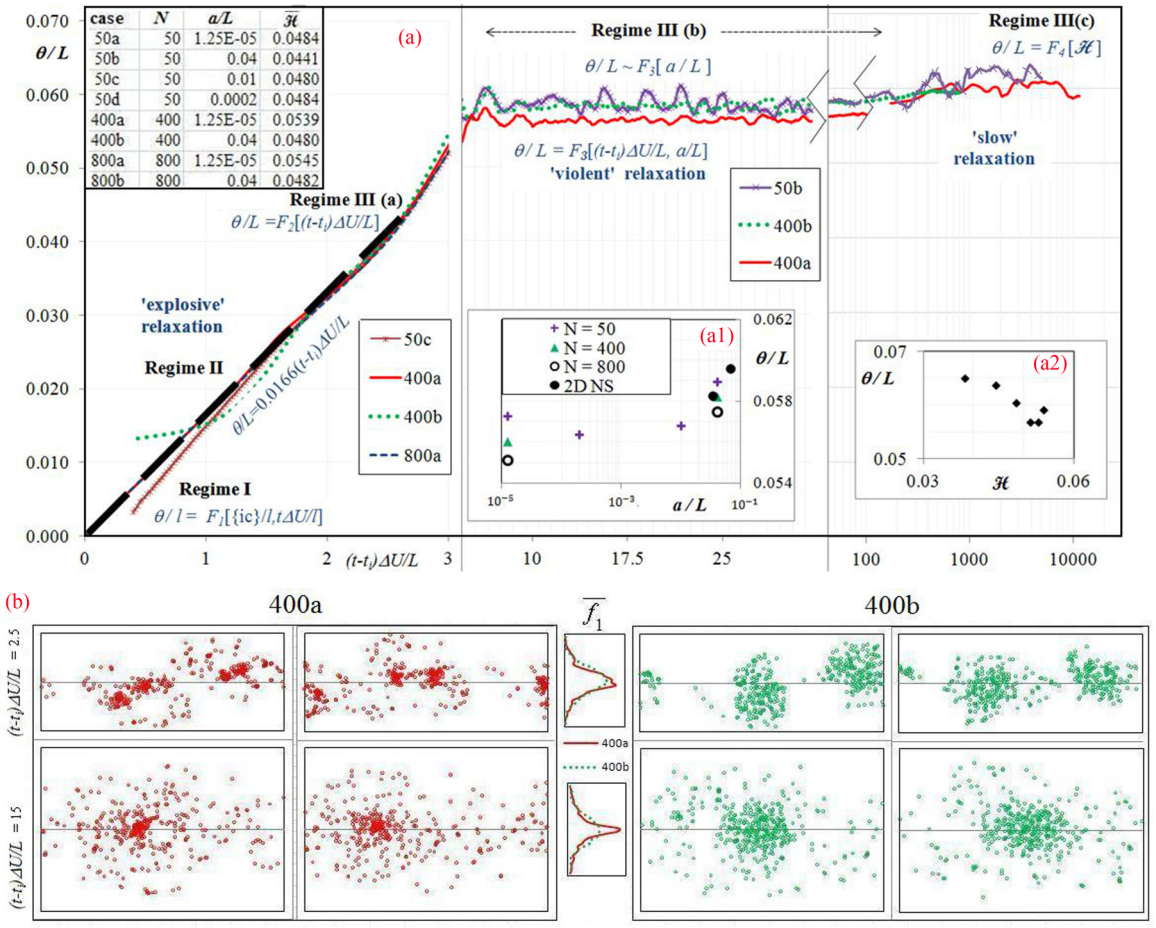

FIG. 13. (Color online) (a) Complete evolution of shear layer thickness, showing subregimes of Regime III and their relation to Regimes I and II for different initial conditions and N. [In order to optimize computational effort, large member ensemble averages have been used for Regimes I, II, and III(a) and a combination of ensemble and short time averaging has been used at later times; data for $t\Delta U/L > 10^3$ are from single realizations.] (b) Distribution of vortices within "structures" in Regimes III(a) (top row) and III(b) (bottom row), with "gentle" (case 400a) and "highly disturbed" (case 400b) initial conditions.

Figure 13(b) shows a snapshot of vortex locations for cases 400a and 400b (with two different realizations in each case), both having the same number (400) of vortices but initial y displacements drawn from uniform random distributions of widely different amplitudes, $1.25 \times 10^{-5}L$ (to be called the "gentle" case) and $0.04L$ ("highly disturbed" stronger case), respectively. It can be observed from Fig. 13(b) that, in the left panel, simulations in the gentle case show structures with dense cores, characterized by high concentration of vortices. With highly disturbed initial disturbances (right panel, 400b) the cores are not so dense.

From the snapshots in the top panel in Fig. 13(b), at $t\Delta U/L = 2.5$ corresponding to an early phase in Regime III(a), it can be seen that the size and relative locations of the two coherent structures present in the domain are similar. Also, there is almost no difference in the x- (and ensemble) averaged single-vortex distribution function $\overline{f_1}$. This suggests that the averaged vorticity and velocity profiles have only a weak dependence on the distribution of vortices within each coherent structure as compared to the distribution of the coherent structures in the domain. The bottom panel, at $t\Delta U/L = 15$, is discussed in the next section. These observations indicate why the evolution of θ obtained from the x- and ensemble-averaged velocity distribution is universal for different initial-condition classes, whereas the vorticity distribution within a single coherent structure is not. Variations in the y locations of the structures averages out the effect of vorticity distribution within each structure. This also explains the universality of $\overline{f_1}$ in spite of the nonuniversality of f_2' at small $|x_1 - x_2|$ in Regime II shown in Fig. 12.

Regime III(b). Figure 13 shows that, following III(a), the momentum thickness varies very slowly, $((\Delta(\theta/L) < 0.01$ during $4 < t\Delta U/L < 10^4$, a change less than 20% of that seen during $0 < t\Delta U/L < 4)$. Indeed, θ seems to asymptotically approach a constant value. Further, beyond $t\Delta U/L \sim 4$, there is only one structure left in the domain [for evidence, see inset in Fig. 5, also Fig. 13(b)], and the evolution of momentum thickness is no longer universal. We label this subregime III(b).

The lack of universality in Regime III(b) [and subsequently also in III(c)] is consistent with the argument presented above for Regime III(a); namely, the gentler initial conditions lead to higher vortex density in the core of the structure. It can be seen from Fig. 13(b) that, in contrast to III(a), III(b) shows significant differences in $\overline{f_1}$, which has a tall narrow peak at the center, showing the small dense cores in the gentle initial condition case. Since III(b) involves a single structure, and since the y centroid is invariant in time, the ordinate of the core of the structure would be similar in different realizations. Hence, unlike in Regimes II and III(a), an altered distribution of vorticity within the structure does affect the ensemble-averaged statistics. This explanation is consistent with the observation of lower thickness for the gentler initial conditions in Regime III(b), shown in Fig. 13(a). Further, the early part of III(b) follows Euler dynamics under certain limits, and the thickness is a function of only a/L, as shown in the inset. This is discussed further when we compare the present results with Navier-Stokes solutions in Sec. VII.

Regime III(c). We label the statistically stationary asymptotic state $(t\Delta U/L \to \infty)$ III(c). In the present simulations

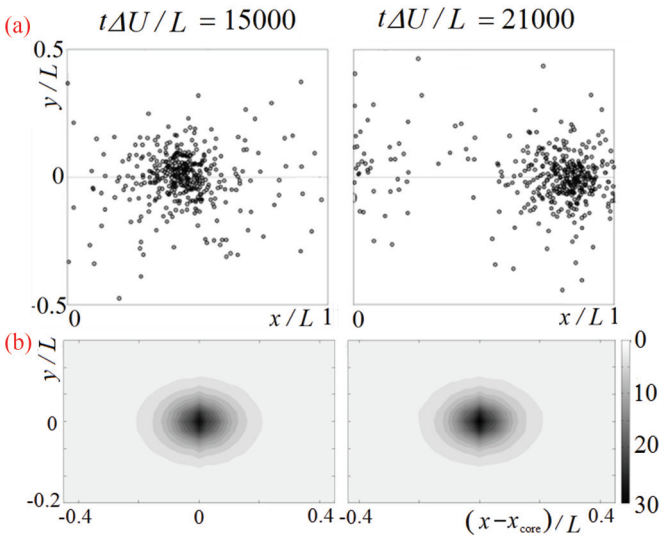

FIG. 14. (Color online) (a) Vortex positions in Regime III(b) at times $t\Delta U/L = 15\,000$ (left) and 21 000 (right). (b) The single vortex distribution of $(x - x_{\rm core}, y)$ at $t\Delta U/L = 15\,000$ and 21 000, averaged over $250L/\Delta U$. Note invariance with time.

with $N = 400$, this state appears to be attained (for all practical purposes) when $t\Delta U/L > 10^4$.

To study this regime, very long-time simulations ($t\Delta U/L$ up to 3×10^4) have been performed, with N ranging from 50 to 400. Figure 14(a) shows snapshots of the vortex locations at two different times, respectively, 15 000 and 21 000 $L/\Delta U$. It can be seen that at both times there is a single structure with a similar configuration of vortices within the structure, but the structure itself is found at different x locations. The lone structure in the domain, in fact, keeps moving back and forth in x, sampling the entire domain over time scales of $O(10^3 L/\Delta U)$. Figure 15(a) shows the time series of the position of the core of the structure. (The core represents the zone of highest vortex density, and its position is taken as the x location $x_{\rm core}$ of the vertical strip with the highest number of vortices, out of 101 vertical strips of equal width over the domain.) On the right in Fig. 15(a) the histogram representing the probability density function (PDF) of $x_{\rm core}$ shows that it samples the entire domain with roughly equal probability. This is consistent with ergodicity because, unlike in the case of the infinite plane, the x centroid (in the sense it has been used in this paper) of the present x-periodic system is not conserved [however, $(\sum_i x_i) \mathrm{mod} L$ is conserved]. From Fig. 15(b) it is seen that the PDF of the velocity of the core does not change with time beyond $15\,000L/\Delta U$, and appears to agree well with a Gaussian of zero mean. All this evidence confirms that $x_{\rm core}[t]$ tends to a stationary stochastic process in the limit $t \to \infty$ (at any fixed N).

As the size of the structure in the final state scales with L, the effect of boundaries cannot be neglected in III(c) however large the domain may be. This shows that the common argument about a final state independent of the boundary conditions, widely used in much of statistical mechanics, is not applicable to the problem of determining the final state of the present system involving long-range interactions.

However, according to Fig. 15(a) the number of crossings of $x = 0.5L$ with $N = 400$ is roughly half that at $N = 50$, so

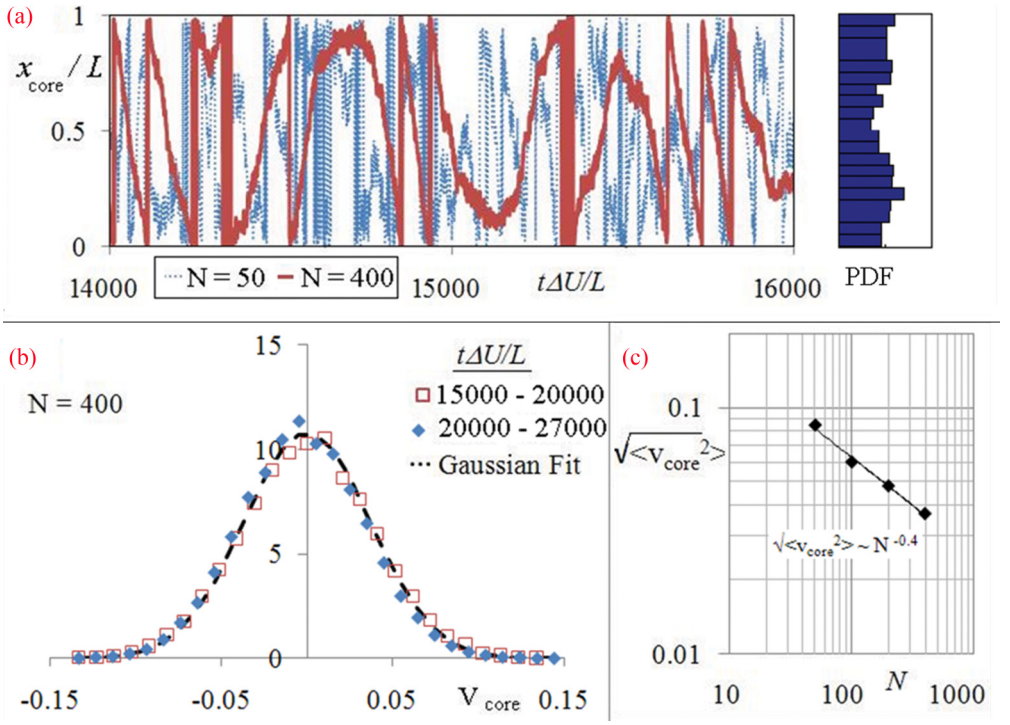

FIG. 15. (Color online) (a) Motion of the core of the structure in Regime III(b). The solution samples all x-translated states but with very long time scales that increase with increase in number of vortices. Also shown is a histogram of the locations sampled by the core over $t = 15\,000$–$27\,000 L/\Delta U$ for $N = 400$. (b) The motion of the core relaxes to a stationary stochastic process as can been seen from the PDF of a characteristic velocity (defined as the distance moved by the core as a fraction of the domain during one $L/\Delta U$). (c) The velocity of the core decreases with increasing number of vortices as $N^{-0.4}$.

the time taken by the structure for crossing the L domain is twice as long at the higher value of N. From Fig. 15(c), the standard deviation of a characteristic velocity of the structure decreases like $N^{-0.4}$. Thus, if the limit $N \to \infty$ is taken first, the possibility that the structure may be stationary as $t \to \infty$ cannot be ruled out. The final asymptotic state, as well as ergodic behavior in x, could therefore depend on the order in which the limits $t \to \infty$ and $N \to \infty$ are taken (as pointed out by Chavanis [11] in the more generalized context of vortex-gas statistical mechanics).

Reverting to the limit $t \to \infty$ of an N-vortex system, we now study the distribution of the vortices within the structure relative to the (moving) center. We carry out a "short-time average" (over a duration of $250 L/\Delta U$) of the location of vortices around the core at 15 000 and 21 000 $L/\Delta U$. This is shown in Fig. 14(b). It is seen that there is very little variation between the single-vortex distributions across the two times. Further, as the orientation of the oval shape does not change, the structure as a whole is not in solid body rotation, but the individual vortices are in relative motion with respect to each other, as, for example, in density wave motion in galaxies.

This leads to perhaps the most important question in the statistical-mechanical analysis of any system, namely whether a state of equilibrium (relative to a moving structure) exists, and, if so, whether it has been reached or not at any given time. A necessary but not sufficient condition for the system to be in equilibrium is that molecular chaos should have set in; more precisely, the two-point correlation functions f_2' must vanish in the thermodynamic limit $N \to \infty$. That would be consistent with all higher order correlation functions also tending to zero. This question is specifically addressed in Fig. 16. It is

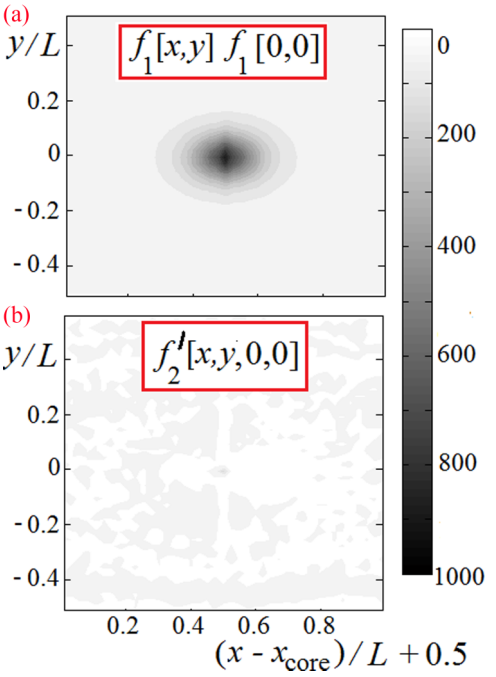

FIG. 16. (Color online) Comparison of distribution functions for vortices relative to the center in Regime III(c) (averaged over $t\Delta U/L = 15\,000$–$27\,000$).

seen that f_2' computed from the time-averaged statistics in the frame of reference of the moving structure [Fig. 16(b)] is small compared to $f_1 * f_1$ [Fig. 16(a)]. Thus, molecular chaos ($f_2 = f_1 * f_1$) should be a reasonable assumption in attempts to analyze the statistics of the distribution of vortices within the moving structure. A comparison may be made with the same distribution function in Regime II, where the difference $f_2 - f_1 * f_1$ was found to be significant (Figs. 11 and 12).

Now we turn to the necessary and sufficient conditions for equilibrium: The single-particle distribution must be independent of time and be governed by a single parameter, namely the temperature or its equivalent. The time independence has already been satisfactorily demonstrated in Fig. 14(b). The temperature may be estimated based on the results of Joyce and Montgomery [57] and Chavanis [55]. According to them, equilibrium is described by the single-vortex Boltzmann distribution

$$\frac{\Delta U}{L} f_1 \equiv \langle \omega \rangle = A \exp[-B\psi],$$

where $B = \rho\beta\gamma$, ρ is a density (not necessarily that of the fluid), $\beta = 1/(k_B T)$, k_B is the Boltzmann constant and ψ is the stream function defined by $u = \partial\psi/\partial y, v = -\partial\psi/\partial x$.

The averaged stream function at the ith box, $\psi[i]$, can be computed numerically from the computed discrete values of f_1 using the expression (easily derived from Eqs. (1) and (2) and the definition of ψ and f_1)

$$\psi[i] = -\frac{\Delta U}{L}\frac{1}{4\pi}\sum_{i\neq j} f_1[j] \ln\left(\frac{1}{2}\left\{\cosh\left[\frac{2\pi(y_i - y_j)}{L}\right] - \cos\left[\frac{2\pi(x_i - x_j)}{L}\right]\right\}\right)\Delta x \Delta y.$$

For the present simulation of case 400a, it is seen from Fig. 17 that the ψ-ω relationship in Regime III(c) follows the Boltzmann distribution for $f_1 > 0.03$. The value of B, estimated by best fit to the time-averaged data, is $-24.3/(\Delta U L)$, so

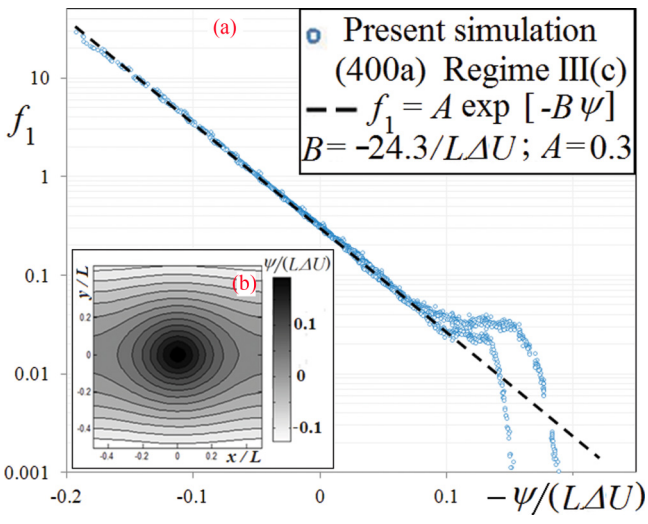

FIG. 17. (Color online) (a) The stream function-vorticity relation in the frame of the moving structure in Regime III(c) (averaged over $t\Delta U/L = 15\,000$–$27\,000$) for case 400a. (b) Contour plot of the stream function for the same.

$\beta = -24.3/\rho N\gamma^2$. (The two seemingly distinct branches for $f_1 < 0.03$ in Fig. 17 correspond to data from the top and bottom of the layer, implying some up-down asymmetry, but this is expected to disappear with sufficiently long averaging.)

Since $\langle\omega\rangle \equiv -\nabla^2\psi$, a partial differential equation can be written for the stream function [57] using as source density the Boltzmann distribution for f_1,

$$-\nabla^2\psi = A \exp[-B\psi]. \tag{14}$$

A closed-form solution of the above equation was derived by Lundgren and Pointin [6] for the infinite plane, but none has been reported so far under the present boundary conditions. One interpretation of the present results emerges from a comparison of the distribution function obtained numerically here for the shear layer with the Lundgren-Pointin solution for the infinite plane,

$$P[r/R_0] = \frac{\tilde{A}\exp[-(1+\lambda)(r/R_0)^2]}{[1 - \pi\lambda\tilde{A}(r/R_0)^2]^2}. \tag{15}$$

Here r is the radial distance from the centroid, R_0 is the radius of gyration, $\lambda = \rho N\gamma^2\beta/(8\pi)$, and $\tilde{A}$ is a normalization constant that ensures $\int_0^\infty 2\pi r P[r]dr = 1$. Some words of caution are, however, necessary here as the infinite plane problem studied by L-P has the Hamiltonian given by Eq. (3), which is clearly different from the present Hamiltonian given by Eq. (4). The conserved quantities are also different in the two cases.

A value for λ can be determined by making a best fit to the L-P distribution function (18). As seen in Fig. 14(b), the vortex distribution in the present problem is not isotropic, because of periodicity only along the x direction and a domain that extends to $\pm\infty$ in y. To analyze the distribution, we perform sectorwise averaging in the x-y plane and renormalize with the number of vortices in the respective sector. We then find that the radial distribution of vortices in each of the three distinct sectors shown in Fig. 18 approximately follows a truncated Lundgren-Pointin distribution, with λ (determined by best fit) taking the values -0.972, -0.985, and -0.9884 as we move from the sector covering the x axis to that covering the y axis. With the use of the present nonangular description for x, the distribution function also gets truncated. We note that the values of λ thus obtained are close to -1, the lowest value allowed by L-P. This could be due to the present initial conditions, wherein the vortices are concentrated in a thin strip, which result in high energy configurations that lead to negatively high temperatures.

The inverse temperature β takes values of $-24.46/(\rho N\gamma^2)$, $-24.79/(\rho N\gamma^2)$, and $-24.84/(\rho N\gamma^2)$ in the three sectors, respectively, going counterclockwise from x to y axes. Further, we find that λ based on the LP relation between scaled energy and λ is $-0.999\,99$ and hence the corresponding $\beta = -25.167/(\rho N\gamma^2)$. These values are very close to the value of $-24.3/(\rho N\gamma^2)$ earlier determined for β using the ψ-ω relationship. This shows that the temperature of the present vortex-gas system, regardless of the method of estimation, is negative, corroborating the seminal idea of Onsager, namely the connection between negative temperature states and emergence of order in the form of coherent structures.

Onsager did not deal explicitly with questions of the thermodynamic limit in his paper, but they are important for the statistical mechanics of the vortex gas. Frohlich and Ruelle [60] carried out a rigorous analysis of a neutral vortex gas for the case in which the energy grows linearly with N when individual vortex strengths are held fixed. (While energy formally scales as N^2, the N^2 terms were assumed to cancel out [60] for the neutral case and thus energy may scale as N. However, this need not be the case when the positive and negative vortices separate). Frohlich and Ruelle studied the limit $N \to \infty$ with the average energy per particle E/N and the number density N/A (A is the area of the domain) held fixed without any scaling of γ. They showed that in such a formulation there are no negative temperatures in the thermodynamic limit. Eyink and Spohn [7] showed that for obtaining negative temperatures energies that scale as N^2 must be considered. Eyink and Sreenivasan [8] present a review and discussion on the above issues, and state that a nontrivial limit with energy of $O(1)$ can be obtained only if $\gamma \sim O(1/N)$. This limit has often been adopted, including in some recent studies [11]. Note that in all of the above mentioned studies, ρ is kept fixed.

In the free shear layer problem all the vortices are of the same sign, and hence there is a well defined total circulation prescribed by the fluid dynamics. Hence, the natural limit is $N \to \infty, \gamma \to 0$, with $N\gamma = L\Delta U$ fixed, as it recovers the continuous vorticity distribution of a temporal shear layer in a given domain L and with a prescribed velocity difference ΔU. Thus, both L and ΔU, fixed by the underlying fluid-dynamical problem, are independent of N.

If we also adopt the conventional fluid-dynamic definition of energy given by $E = \rho_l H$, where ρ_l is the density of the fluid (which is independent of the properties of the vortex gas), the energy scales as $(L\Delta U)^2$ and hence is

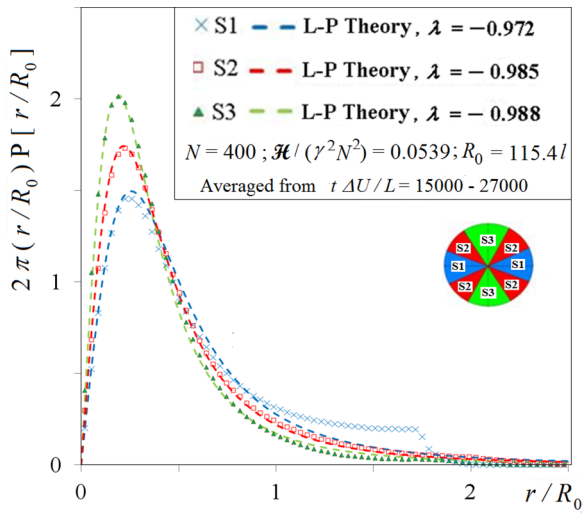

FIG. 18. (Color online) Sector-averaged radial (core-centered) distribution function in Regime III. Each sectorwise distribution function is similar to a Lundgren-Pointin equilibrium type but of different "temperature." R_0 is the initial value of the second moment. Note that the sectors are chosen only for illustration and numerical convenience and that the "temperature" is expected to continuously vary with $\tan^{-1}[x/y]$.

N independent and nonextensive (in N). This leads to the temperature scaling as $\rho_l N\gamma^2 = \rho_l (L\Delta U)^2/N$, which is N dependent and goes to zero in the thermodynamic limit. This is an expected consequence of a nonextensive energy but an extensive entropy. Adopting the fluid dynamically relevant limits therefore leads to "strange thermodynamics."

However, we must note that just as the temperature of the vortex-gas system (which could be negative) is not related to the temperature of the fluid (which is strictly positive), the energy of the vortex-gas system is not directly related to the energy of the fluid. This also implies that the density in the expressions for energy and temperature need not be related to the density of the fluid. Therefore, one is free to determine an appropriate "density" for the vortex gas. To do this, we revisit Hamilton's equations [Eq. (5)] and recast them in a form in which the respective quantities have the usual dimensions of position, momentum, and energy,

$$\frac{dX_i}{dt} = \frac{\partial E}{\partial Y_i}, \quad \frac{dY_i}{dt} = -\frac{\partial E}{\partial X_i}, \tag{16}$$

with positions $X_i = x_i$, momenta $Y_i = \mathcal{A} y_i$, and energy $E = \mathcal{H}$, where $\mathcal{A}$ is a constant factor that provides Y_i the units of momentum and has units of density, so that E has the units of energy. Any rescaling of x_i and y_i by γ-dependent factors implies that such a scaling would be sensitive to the particular limits chosen, and a clear discussion is not straightforward. For the Biot-Savart equations (1) and (2) to be recovered, $\mathcal{A}$ should be set to $\gamma\rho$. Since $\mathcal{A}$ is a constant factor, $\rho \sim 1/\gamma$. This density does not have a direct physical interpretation (as it is related to neither the number density of the vortices nor the density of the fluid) and only ensures that the transformed quantities in Hamilton's equations for the vortex-gas system have conventional dimensions.

However, if we adopt the above definition of density in the expressions for energy and temperature, we find that in the fluid-dynamically relevant limit $\gamma \sim 1/N$, we have $E = \rho\mathcal{H} \sim (1/\gamma)(N^2\gamma^2) \sim N$. This is an extensive energy function, consistent with standard thermodynamics. Temperature scales as $\rho N\gamma^2 \sim N\gamma$, which is a finite nonvanishing N-independent fixed quantity $L\Delta U$ even in the limit $N \to \infty$. With this definition of density, the fluid-dynamically relevant limits are also consistent with standard thermodynamics, and under these limits our simulation results when combined with the Joyce-Montgomery relation also point to the temperature having a linear dependence on $L\Delta U$.

We now make a few brief remarks on the issue of recurrence. While the Poincaré theorem suggests reversibility, it is well known in statistical mechanics that the recurrence times often increase exponentially with N and can be astronomical for large-N systems [61]. Hence, such a recurrence is not expected to be observed in any realistic-time calculation involving a reasonable value of N. However, since Birkhoff and Fisher [48] suggested that a vortex sheet (discretized using point vortices) will eventually unroll following the Poincaré theorem, we briefly explore this issue even though it is not entirely clear whether the theorem applies to this problem. Further, it is unlikely that any numerical scheme could return a system of point vortices to a close vicinity of the initial state even if the Poincare theorem holds, due to nonzero numerical noise (as discussed in Sec. II D). So we explore this issue using a weak

criterion of recurrence, defined by the rms value of y positions of the vortices being within a 20% neighborhood of the initial value. Simulations performed with four to seven vortices show that such a weak recurrence does occur (for single realizations) over very long time scales. For $N = 6$, average recurrence time $t_{\rm rec} \sim 25\,000 L/\Delta U$, and is found to increase exponentially with N. On extrapolation, $t_{\rm rec} \geqslant 10^{64} L/\Delta U$ for $N \geqslant 10^2$, which is 60 orders of magnitude longer than the maximum time of integration in the simulations. Further, instability ensures that such an unrolling is immediately followed by rolling. While we cannot be certain that the final state reached in the present simulations is representative of pure Hamiltonian dynamics, the above findings are not inconsistent with the remarks of Birkhoff and Fisher. Thus, the present observation of the average equilibrium thickness being much larger than the initial thickness does not necessarily contradict the argument that rolling has to be followed by unrolling at some point in time. Instead, it only suggests that the time spent in the unrolled states is only a very small fraction of the total time and hence is not reflected in the statistics involving long-time averages.

VII. RELEVANCE TO NAVIER-STOKES MIXING LAYERS

So far, we have considered the vortex-gas shear layer as a prototypical problem in nonequilibrium statistical mechanics in its own right. It is, however, known that under certain conditions discrete point-vortex simulations can tend to smooth solutions of the Euler equations [62,63]. Also, as discussed in the Introduction, the effect of viscosity becomes vanishingly small at high Reynolds numbers in turbulent free shear flows. Furthermore, experiments show that plane mixing layers are dominated by the largely inviscid interaction of quasi-2D coherent structures and that growth occurs through amalgamation of such coherent structures [15,28]. Vortex-gas simulations show the same mechanisms in operation. Therefore, it is of interest to analyze briefly connections with 2D and ("real") 3D Navier-Stokes mixing layers.

A. Regimes I and II: Comparison with laboratory experiments

As the analog of Regime III has never been reported in any experimental study of mixing layers, Regimes I and II are most relevant for comparison with available experimental data. Further, the explosively relaxing Regime II is analogous to the "self-preserving" state [53] in a turbulent shear flow. From dimensional analysis, the growth rate of a canonical 3D Navier-Stokes temporal mixing layer is given by

$$\frac{d\hat{\delta}}{d(t\Delta U)} = F\left[\mathrm{Re}, \{\text{initial conditions}\}\right]. \tag{17}$$

Two major assumptions are introduced at this stage: (i) Any turbulent flow (subject to constant boundary conditions) evolves asymptotically to a state independent of the detailed initial conditions excepting for any integral invariants demanded by mass, momentum, and/or energy conservation, and (ii) "if the equations and boundary conditions admit a self-preserving solution the flow asymptotically tends to that solution." Both hypotheses, while being controversial, are extensively used in turbulent shear flow analyses (see "working rules" (2) and (3) in Ref. [64]).

Such rules imply that, eventually, the initial conditions are "forgotten" as $t \to \infty$ and the effect of Reynolds number becomes vanishingly small at sufficiently large Reynolds numbers. Equation (17) then reduces to

$$\frac{d\hat{\delta}}{d(t\Delta U)} = C_2. \tag{18}$$

The question of whether the constant C_1 is universal in the vortex-gas shear layer is analogous to the controversy on the possible dependence of the self-preservation state of turbulent shear flows on initial conditions [16,54,64–66], i.e., whether C_2 is a universal constant.

Sinusoidally perturbed mixing layers (referred to as "periodically forced" mixing layers in the fluid-dynamical literature) provide excellent test cases for comparison with experiments as the dominant initial perturbation is accurately known. Experiments show that sinusoidal perturbations greatly alter the development of the mixing layer, and this has led to strong doubts about universality [16,67]. The perturbation can be imposed in many ways: oscillating the free streams [68], acoustic excitation by loud speakers [69], or periodic deflection of a flapper at the end of the splitter plate [16,70,71]. The last method basically imposes a periodic deflection on a vorticity layer at its origin $x = 0$ [see Fig. 1(c)]. The analog for the temporal vortex-gas shear layer is to have an initial y displacement of vortices that varies sinusoidally with x, as with cases P1 and P2 discussed in Sec. IV.

On this basis, we compare experimental results of the spatial mixing layer reported by Oster and Wygnanski [16] with the present temporal vortex-gas simulations using the Galilean transformation $x = U_m t$. Two such cases are shown in Fig. 19. We compare the evolution of thickness with time, both nondimensionalized using the wavelength of the perturbation as the length scale. The simulations are chosen to have approximately the same value of amplitude to wavelength ratio of the initial perturbation as in the experiment. This implies initializing vortex locations in the simulations as $x_i = N(i/L)$; $y_i = a_w \sin[2\pi x_i/\Lambda] + a_n Y_i$, where Y_i is a random number uniformly distributed between -1 and 1, and $a_w/\Lambda = a_f f/U_m$, where a_f and f are amplitude and frequency of flapper motion in the experiment. We have added a random disturbance a_n to the periodic vortex deflection imposed at $t = 0$ to allow for the presence of tunnel free-stream turbulence and other facility-specific random disturbance sources on the flow. This may also be a proxy for effects due to spatial feedback or three dimensionality.

Figure 19(a) shows the evolution of momentum thickness for $a_w/\Lambda = 0.0074$ for two different values of a_n/a_w. We find from both the simulations that the spreading rate is first enhanced (higher than the Regime II value) and then suppressed, but finally appears to approach the universal spreading rate in Regime II. The vortex-gas simulation with $a_n/a_w = 1.5$ agrees quantitatively with the Oster-Wygnanksi experiment [16] with $a_f f/U_m = 0.0074$ all the way. If a_n/a_w is drastically reduced to 10^{-3}, the simulation still agrees qualitatively with the observed behavior of the mixing layer, but the temporal extent of suppression is longer. Interestingly, addition of the disturbance a_n hardly affects the early evolution of the layer ($t\Delta U/\Lambda < 2$)

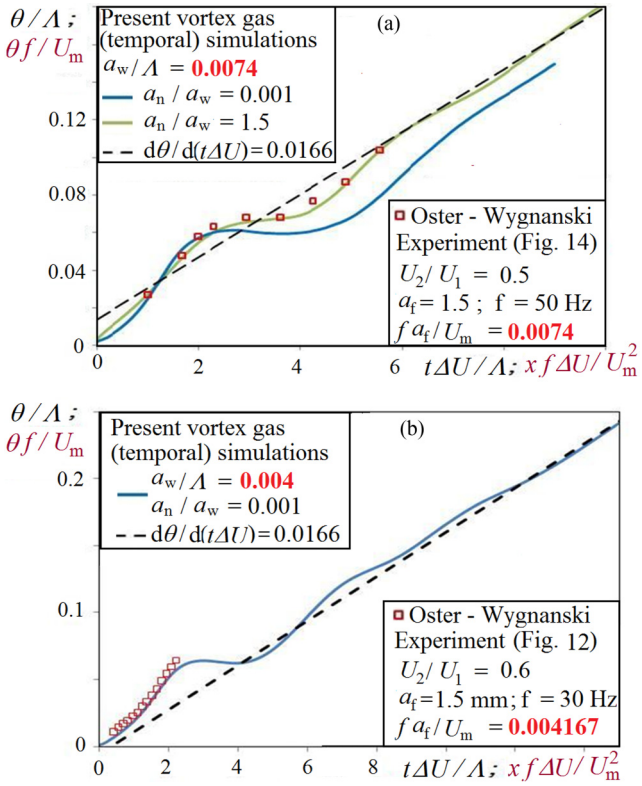

FIG. 19. (Color online) Comparison of temporal evolution of momentum thickness in the present vortex-gas computations with sinusoidal (in x) initial conditions ($t = 0$) with the spatial evolution of momentum thickness in experiments (Oster and Wygnanski, 1982) with sinusoidal (in t) perturbation at $x = 0$.

or the Regime II spreading rate (reached beyond $t\Delta U/\Lambda \sim 8$). The agreement seen in Fig. 19(a) is therefore encouraging.

In Fig. 19(b) we compare the results of case P1 with the experiment with approximately the same amplitude to wavelength ratio. Here the experiments do not go beyond the initial growth-enhancement phase ($t\Delta U/\Lambda < 2$). However, the simulation shows excellent agreement with experiment, but continues into the two later phases, respectively of suppressed growth and recovery towards universality, shown in Fig. 19.

The good agreement of the vortex-gas simulations with the experiment over the range of data available suggests that the attribution of data like those in Fig. 19(a) or 19(b) to lack of universality may not be justified. The obvious interpretation of the experimental data is that introducing strong long-wave periodic perturbations just makes Regime I much longer. Extrapolating from the simulation results of Fig. 19(b) on the time taken to reach Regime II, the distance necessary to reach the equivalent state would be six times as long as the spatial range available in the experimental facility used: the wind-tunnel test section length would have to be increased from 1.5 to about 9.0 m. Further comparisons made with similar experiments reported recently by Naka *et al.* (2010) show agreement almost as good (not shown here). In these studies also, as in Fig. 19(b), the entire experimental region lies in Regime I.

The Regime II universal growth rate found here is within the range quoted across different experiments (0.012 to 0.022) (see [24] and [20]) and Direct Numerical Simulations (DNS) / Large Eddy Simulations (LES) studies of 3D Navier-Stokes temporal mixing layers (0.012 to 0.018). These observations indicate that the conclusions on Regime II drawn from the present vortex-gas study are relevant to real mixing layers. A more detailed analysis of the scatter in the quoted spreading rates will be presented elsewhere.

B. Regime III: Comparison with 2D Navier-Stokes simulations

Although Regime III has not been a subject of any experimental studies, the long-time 2D Navier-Stokes simulations due to Sommeria *et al.* [23] provide a useful benchmark in this context, and a comparison of their results with the present work proves illuminating. They consider a constant-vorticity layer of finite thickness with a piecewise linear velocity profile. This can be represented by a suitable array of point vortices in the Euler limit. One way of defining the relevant vortex-gas initial condition is to have an array of vortices equispaced in x with y displacements from the x axis drawn from a uniform random initial distribution with amplitude a set equal to the half width of the uniform vorticity layer, with $l/a \ll 1$. The comparison is meaningful because, as discussed in the Introduction, a 2D Navier-Stokes solution may also be expected to tend towards a 2D Euler solution at any finite time in the limit $\mathrm{Re} \to \infty$, as does a discrete vortex gas in the limit $N \to \infty$.

We first return to the evolution of the momentum thickness for $t\Delta U/L < 30$ in the present vortex-gas simulations shown in Fig. 13. Sommeria *et al.* [23] present results for evolution of momentum thickness for two different initial half widths, namely $0.017L$ and $0.034L$, at Reynolds numbers $L\Delta U/\nu$ ranging from 9425 to 25133 (750 to 2000 in a definition of $\mathrm{Re} = 1/\nu$ with $L = 2\pi$ and $\Delta U = 2$). Their results show an initially rapid growth of momentum thickness, with slow changes beyond $t\Delta U/L \sim 4$. Since they do not perform ensemble averaging, statistically accurate estimation of spreading rates in Regime II is not possible. However, the situation is different in the slowly varying Regime III as short-time averaging can be carried out to improve the statistics.

It can be seen from Inset (a1) of Fig. 13 and Fig. 20 that at $a/L = 0.04$, the difference in momentum thickness (averaged over 14 to 16 $L/\Delta U$) across $N = 400$, 800, and 1600 is only 1.3%. This suggests that for $N > 400$, the solution hardly depends on N in the vortex-gas simulations, and θ/L is a function only of a/L. From Fig. 20 it is seen that the momentum thickness in Regime III(b1) (to be introduced below) in the present simulations is within 1% of the corresponding value in the 2D Navier-Stokes simulations(case with higher Re of 2000, $a/L = 0.034$).

We next compare the vorticity-stream-function relation in the same two simulations in Regime III(b) characterized by a slowly wandering single structure (in the finite-N vortex-gas simulations). For this purpose, we compute ensemble and short-time averages in a frame of reference fixed with respect to the center of the structure. Further, since ψ is defined up to an additive constant, it is adjusted to 0 at $y = \pm L$ following Sommeria *et al.* Figure 21 compares the ψ-ω relation in the 2D NS with the present vortex-gas simulations. The two

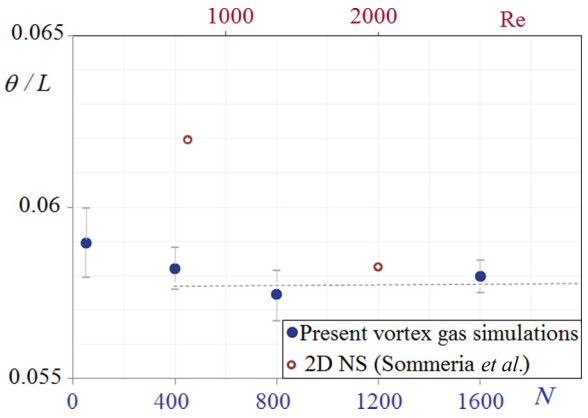

FIG. 20. (Color online) Comparison of momentum thickness in Regime III(b1) (averaged over $t\Delta U/L = 14$ to 16) of the present vortex-gas simulations with $a/L = 0.04$ with 2D Navier-Stokes [23] with $a/L = 0.034$. Error bars show 95% confidence limits and the dashed line shows a possible asymptotic value of thickness.

agree quite closely, over the range $0.05 < \langle\omega\rangle/\omega_0 < 0.5$ at $t\Delta U/L \sim 20$, before viscous dissipation becomes dominant in the NS solution. This agreement indicates that at such times both computations closely follow Euler dynamics.

This result must be considered of great significance, for the close agreement between two such physically and mathematically distinct approaches to the same problem establishes the quantitative relevance of the vortex-gas results to high-Reynolds Navier-Stokes solutions in free turbulent shear flows.

Relation to Euler equilibrium. We now return to a discussion of the equilibrium state. As discussed in Sec. VI, on neglecting correlations (i.e., setting $f_2' = 0$) and taking the limit $t \to \infty$ before the limit $N \to \infty$, the single-particle

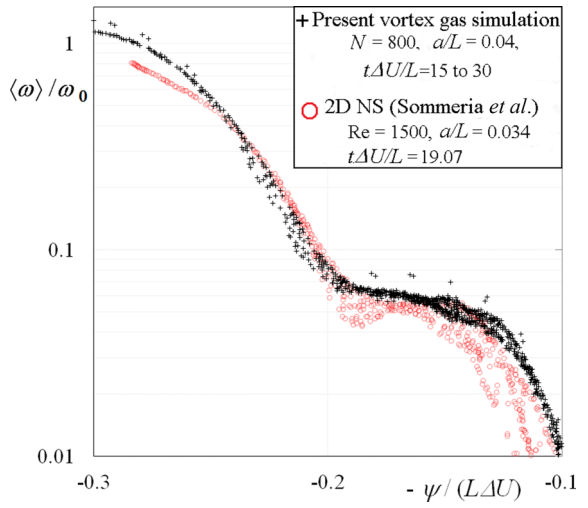

FIG. 21. (Color online) Comparison of the vorticity-stream-function relation between a present vortex-gas computation and 2D Navier-Stokes solution of Sommeria *et al.* [23] at similar parameter values. $\langle\omega\rangle$ is the time-averaged vorticity and ω_0 is the maximum vorticity in the initial condition. In the vortex-gas simulations, $\langle\omega\rangle \equiv f_1 \Delta U/L$ is the ensemble-averaged (coarse grained) vorticity and $\omega_0 = \Delta U/(2a)$.

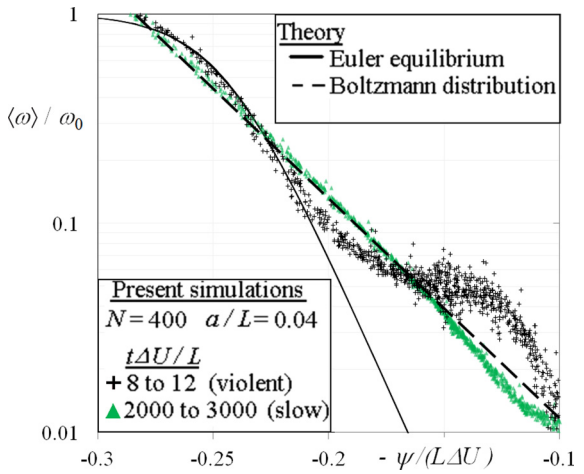

FIG. 22. (Color online) Comparison of present simulations at two times with Euler equilibrium of Robert and Sommeria [58], and the "Boltzmann" distribution of Onsager/Chavanis. Note that both theoretical curves are two-parameter fits, and the averaging in the present simulation has been done relative to the center of the structure.

distribution at statistical equilibrium for a point vortex gas [32] (also see [55]) is shown to be characterized by the Boltzmann distribution. It is obtained by maximization of $-\int f_1 \ln[f_1]$, subject to the constraint of Hamiltonian conservation, and is given by $f_1 \sim \exp[-B\psi]$, where the Lagrange multiplier B can be interpreted in terms of an inverse temperature.

On the other hand, it has been proposed by Robert and Sommeria [58] that an "equilibrium state" for Euler flow is obtained through maximization of the Kullback entropy,

$$-\int (f_1 \ln[f_1] + (1 - f_1)\ln[1 - f_1]).$$

Here f_1 is scaled with its maximum value in the initial condition, subject to constraints of kinetic energy and linear and angular momentum of the Euler flow. This limit is expected to be reached if the limit $N \to \infty$ precedes the limit $t \to \infty$ [11]. This theory was applied to determine the final state of a temporal shear layer in an Euler fluid [23] and compared with the 2D Navier-Stokes simulations described earlier.

The present results, shown in Fig. 22, suggest that the vortex gas has a tendency to relax to the Robert-Sommeria Euler equilibrium at "intermediate times" of $O(10L/\Delta U)$, and to the Boltzmann-type equilibrium at much longer times of $O(10^2 - 10^4 L/\Delta U)$ for $N = 400, a/L = 0.04$. We may label these two subregimes of relaxation as III(b1) and III(b2). This is not inconsistent with theoretical results [11,72], which suggest that relaxation to equilibrium in a vortex gas has two stages, namely a "violent relaxation" that closely approximates Euler dynamics and a "slow relaxation" driven by finite-N effects that appear at time scales of $O(N \log N)$, beyond which the vortex gas will relax to the Boltzmann distribution. However, the values of $N < 10^3$ used in these long-time simulations are not large enough for a strict comparison with the proposed Euler equilibrium which is valid only at sufficiently large N, when the time at which finite-N effects become important is much longer than that required for

relaxation to Euler equilibrium. The same limitation applies for a rigorous verification of the proposed $N \log N$ scaling. (Note that for the case considered in Fig. 22, $N \ln N \sim 2400$ and $(Na/L)\ln[Na/L] \sim 45$.)

VIII. CONCLUDING REMARKS

We have here uncovered, through extensive simulations, certain remarkable properties of the statistical evolution of a vortex-gas shear layer from a prescribed initial condition to a final asymptotic state. The present simulations reveal the spontaneous emergence of large-scale order in the form of coherent structures as in earlier studies, but also the existence of three distinct regimes in the evolution and their respective scaling laws. We find that evolution in Regime I depends strongly on initial conditions, Regime II exhibits a universal linear growth in layer thickness with time, and Regime III is a domain-dependent evolution to a final state that involves a single cluster of vortices after violent and slow relaxations [with outer time scales of $O(10)$ and $O(10^4)$, respectively]. The ψ-ω relationship in the vortex gas agrees with that found in the 2D Navier-Stokes calculations during the violent relaxation phase, suggesting that the vortex gas and the 2D Navier-Stokes solutions approach the 2D Euler shear layer from different directions. This also confirms that the vortex-gas model provides a weak solution of the 2D Euler equations [63]. The distribution of vortices within the randomly moving structure reached at the end of the slow relaxation can be roughly described by a truncated, anisotropic variant of the Lundgren-Pointin distribution, and the ψ-ω relationship approaches the Boltzmann distribution for the vortex gas, hence constituting a "relative" equilibrium in the sense defined by Newton [5]: Namely, the distribution is time-invariant relative to the center of a nonstationary structure.

A major finding in this work is the universality of the spreading rate (0.0166 ± 0.0002 for the momentum thickness) of the vortex-gas shear layer in the intermediate Regime II, across a wide range of initial conditions and domain sizes. We show that vortex-gas kinetic theories inspired by the Boltzmann equation are not applicable in Regime II, as they do not account for the strong correlations due to multiple, interacting coherent structures of vortices. This regime lasts for just $t\Delta U/L = O(1)$, an order of magnitude shorter and more intense than the violent relaxation process that occurs in the early stages of Regime III, and can therefore be justifiably called an explosive phase. Regime II is the counterpart of the self-preserving flow regime observed in laboratory experiments of turbulent shear flows in the sense that both mean velocity and Reynolds shear stress profiles exhibit self-similarity with the same velocity and length scales (ΔU and θ in the present case) in the regime. Flows with such self-similarity are often said to be in a state of "equilibrium" in the fluid-dynamical literature (following Clauser [73]). It is ironic that what represents equilibrium in fluid dynamics occurs in what is an early explosive phase of relaxation in nonequilibrium statistical mechanics.

From a fluid-dynamics perspective, the close agreement between the evolution of momentum thickness in the present simulations for periodic initial conditions on the one hand and the observed behavior of spatially developing mixing layers in laboratory (Navier-Stokes) experiments with equivalent periodic forcing on the other is highly significant. Further, the Regime II growth rate of the vortex-gas shear layer is within the scatter of the quoted "self-preservation" spreading rates, across several mixing layer experiments as well as 3D Navier-Stokes simulations. These results suggest that the momentum dispersal in the (Navier-Stokes) turbulent mixing layer is dominated by what may be called the Kelvin/Biot-Savart mechanism at high Reynolds numbers (Kelvin's theorem provides the dynamical justification for considering nondiffusive point vortices whose strength remains the same, and the evolution of the collection of such vortices can be understood via the purely kinematic Biot-Savart relationship). This also supports the argument that strictly 2D approximation of the vortex-gas approach is not unduly restrictive for determining layer growth, as the coherent structures in plane mixing layers tend to be quasi-2D. Further, this is also consistent with the conclusions of the nonlinear calculations of Corcos and Sherman [74] and Corcos and Lin [75], who show that 3D instabilities are inhibited by the growth of the 2D instabilities and are slow growing relative to the 2D coherent-structure amalgamations. These considerations suggest that the present results may be relevant to the long-standing controversy of universality or otherwise of the self-preservation ("fluid-dynamical equilibrium") spreading rates of turbulent shear flows. Some experiments report that an effect of initial conditions on the spreading rate is present over the whole extent of the flow investigated [16,76–78]. However, one cannot, on the basis of such experiments, conclude that the effects will persist "forever." In any case, there are also other studies which have shown that a unique self-preservation state is indeed reached after long transients. For example, we may consider the single-stream shear layer experiments of Kleis and Hussain [79] (figure reproduced in Ref. [64]), conducted in a 12-ft-long chamber. The authors found that the spreading rates of two mixing layers, evolving, respectively, from a laminar or a turbulent boundary layer at the trailing edge of a splitter plate, continue to exhibit differences until approximately 5 ft, after which they both attain the same spreading rate. The present vortex-gas simulations are consistent with the above example in emphasizing that the memory of initial conditions can be extraordinarily long for some initial conditions, but is finite in all the cases considered at least in the 2D problem. This is entirely consistent with the conclusion based on 2D wake flows by Narasimha and Prabhu [54]. Comparison of the present simulations with the experiments of Oster and Wygnanski [16] and Naka *et al*. [71] suggest that, in many of their experiments, the entire flow in the apparatus may have never gone beyond what we identify here as Regime I. This result provides a part of the explanation for the scatter among the quoted "self-preservation" spreading rates in the fluid-dynamics literature. Other possible explanations of the scatter in the quoted spreading rates, especially across DNS/LES studies of temporal mixing layers, include insufficient averaging and estimation of Regime II spreading rates by fits extending to what is actually the domain-affected Regime III. A detailed discussion of this issue will be presented elsewhere.

From a statistical-mechanics point of view, many of the present results could be more generally valid for other multi-scale nonlinear systems with long range interactions, such as

those in plasma and stellar dynamics. The most interesting statistical-mechanics finding here may be the universality of the exponent (=1) as well as the coefficient (=0.0166) in the growth of layer thickness $\theta = 0.0166(t\Delta U)^1 + \text{const.}$ with time during a highly correlated explosive relaxation that is far from statistical-mechanical equilibrium. While the universality of exponents is well known in the theory of critical phenomena, the universality of the multiplying coefficient found in the present system over a vast range of initial-condition classes is at least unusual. The present results may therefore have a special significance in nonequilibrium statistical physics.

ACKNOWLEDGMENTS

We thank Prof. Garry Brown (Princeton) and Prof. Anatol Roshko (Caltech) for many rewarding and enjoyable discussions and suggestions; Prof. Uriel Frisch (CNRS, Nice), Prof. N. Kumar (RRI, Bangalore), and Prof. Joel Sommeria (LEGI, Grenoble) for their comments; and Dr. Ansumali (JNCASR) for suggesting bimodal initial conditions. We are grateful to Dr. S. D. Sherlekar and Dr. R. K. Lagu for providing supercomputing resources on the Tata EKA in the early stages of this study and at Intel more recently. We also thank S. Sapre (TCS) and R. K. V. Malladi (Intel) for assistance in parallelizing and managing computer resources for running our code respectively. We acknowledge support from DRDO through the project RN/DRDO/4124 and from Intel through project RN/INTEL/ 4288. S.S. wishes to thank Dr. Anubhab Roy and Dr. Sourabh Diwan (JNCASR) for discussions. N.D.H. thanks S. K. Vikas for many important discussions about the vortex gas and also for extensive GPU simulations. He acknowledges support from the DST project IR/S2/PU-001/2008.

[1] L. Onsager, Il Nuovo Cimento **6**, 279 (1949).
[2] J. Miller, Phys. Rev. Lett. **65**, 2137 (1990).
[3] E. A. Novikov and Iu. B. Sedov, Zh. Eksp. Teor. Fiz. **75**, 868 (1978) [Sov. Phys. JETP **48**, 440 (1978)].
[4] H. Aref, Annu. Rev. Fluid Mech. **15**, 345 (1983).
[5] P. Newton, *The N-vortex Problem: Analytical Techniques* (Springer, Berlin, 2001), Vol. 145.
[6] T. Lundgren and Y. Pointin, J. Stat. Phys. **17**, 323 (1977).
[7] G. Eyink and H. Spohn, J. Stat. Phys. **70**, 833 (1993).
[8] G. Eyink and K. Sreenivasan, Rev. Mod. Phys. **78**, 87 (2006).
[9] H. Marmanis, Proc. R. Soc. London A **454**, 587 (1998).
[10] P.-H. Chavanis, J. Stat. Mech.: Theory Exp. (2010) P05019.
[11] P.-H. Chavanis, Physica A **391**, 3657 (2012).
[12] J. Miller, P. B. Weichman, and M. C. Cross, Phys. Rev. A **45**, 2328 (1992).
[13] P.-H. Chavanis, Phys. D (Amsterdam, Neth.) **200**, 257 (2005).
[14] H. Liepmann and J. Laufer, National Advisory Committee for Aeronautics Technical Note No. 1257 (1947).
[15] G. Brown and A. Roshko, J. Fluid Mech. **64**, 775 (1974).
[16] D. Oster and I. Wygnanski, J. Fluid Mech. **123**, 91 (1982).
[17] C. Li, K. Chang, and M. Wang, Exp. Therm. Fluid Sci. **33**, 527 (2009).
[18] N. Li, E. Balaras, and J. Wallace, Flow, Turbul. Combust. **85**, 1 (2010).
[19] V. Parezanovic, J. Delville, C. Fourment, L. Cordier, B. Noack, and T. Shaqarin, Bull. Am. Phys. Soc. **57**, H25.00008 (2012).
[20] C. Winant and F. Browand, J. Fluid Mech. **63**, 237 (1974).
[21] J. Liu, Annu. Rev. Fluid Mech. **21**, 285 (1989).
[22] G. L. Brown and A. Roshko, J. Turbul. **13**, 1 (2012).
[23] J. Sommeria, C. Staquet, and R. Robert, J. Fluid Mech. **233**, 661 (1991).
[24] M. Rogers and R. Moser, Phys. Fluids **6**, 903 (1994).
[25] J. Pedlosky, *Geophysical Fluid Dynamics* 2nd ed. (Springer, Verlag, New York, 1987).
[26] G. K. Batchelor, Phys. Fluids **12**, II-233 (1969).
[27] R. Kraichnan, Phys. Fluids **10**, 1417 (1967).
[28] I. Wygnanski, D. Oster, H. Fiedler, and B. Dziomba, J. Fluid Mech. **93**, 325 (1979).
[29] A. Chorin, J. Fluid Mech. **57**, 785 (1973).
[30] B. Delcourt and G. Brown, in *2nd Symposium on Turbulent Shear Flows* (Imperial College, London, 1979), Vol. 1, p. 14.
[31] H. Aref and E. Siggia, J. Fluid Mech **100**, 705 (1980).
[32] D. Montgomery and G. Joyce, Phys. Fluids **17**, 1139 (1974).
[33] O. Bühler, Phys. Fluids **14**, 2139 (2002).
[34] A. Friedmann and P. Poloubarinova, Rec. Géophys., Tome V, Fascicule II, Leningrad **5**, 9 (1928).
[35] L. Rosenhead, Proc. R. Soc. London Series A **134**, 170 (1931).
[36] G. Kirchhoff, *Vorlesungen über Mathematische Physik. Mechanik* (Druck und Verlag von BG Teubner, Leipzig, 1876).
[37] E. Acton, J. Fluid Mech. **76**, 561 (1976).
[38] S. I. Sohn, D. Yoon, and W. Hwang, Phys. Rev. E **82**, 046711 (2010).
[39] M. Abid and A. Verga, Phys. Rev. E **84**, 026318 (2011).
[40] R. Krasny, J. Comput. Phys. **65**, 292 (1986).
[41] F. Hama and E. Burke, Univ. of Maryland Tech. Note BN-220, USA (1960).
[42] D. Moore, California Institute of Technology Report AFOSR-1084-69 (1971).
[43] D. Moore, SIAM J. Sci. Stat. Comput. **2**, 65 (1981).
[44] D. Moore, Proc. R. Soc. London A. Math. Phys. Sci. **365**, 105 (1979).
[45] A. Leonard, J. Comput. Phys. **37**, 289 (1980).
[46] S. Suryanarayanan and R. Narasimha, Bull. Am. Phys. Soc. **55**, LE.00004 (2010).
[47] R. Krasny, J. Fluid Mech **167**, 65 (1986).
[48] G. Birkhoff and J. Fisher, Rend. Circolo Mat. Palermo **8**, 77 (1959).
[49] C. Millikan, in *Proceedings of the 5th International Congress on Applied Mechanics*, edited by J. P. D. Hartog and H. Peters (J. Wiley & Sons, New York, 1939), Vol. 386.
[50] A. Kolmogorov, Dokl. Akad. Nauk SSSR **30**, 299 (1941).
[51] K. Gersten, *IUTAM Symposium on Asymptotic Methods for Turbulent Shear Flows at High Reynolds Numbers: Proceedings of the IUTAM Symposium Held in Bochum, Germany, June 28–30 1995* (Kluwer Academic, Dordrecht, 1996), Vol. 1995.

[52] M. Van Dyke, *Perturbation Methods in Fluid Mechanics* (Academic Press, New York, 1964).
[53] A. Townsend, *The Structure of Turbulent Shear Flow* (Cambridge University Press, Cambridge, UK, 1980).
[54] R. Narasimha and A. Prabhu, J. Fluid Mech. **54**, 1 (1972).
[55] P. H. Chavanis, Phys. Rev. E **64**, 026309 (2001).
[56] M. M. Sano, Phys. Rev. E **76**, 046312 (2007).
[57] G. Joyce and D. Montgomery, J. Plasma Phys. **10**, 107 (1973).
[58] R. Robert and J. Sommeria, J. Fluid Mech **229**, 291 (1991).
[59] D. Lynden-Bell, Mon. Not. R. Astron. Soc. **136**, 101 (1967).
[60] J. Fröhlich and D. Ruelle, Commun. Math. Phys. **87**, 1 (1982).
[61] S. Chandrasekhar, Rev. Mod. Phys. **15**, 1 (1943).
[62] J. T. Beale and A. Majda, Math. Comput. **39**, 29 (1982).
[63] C. Marchioro and M. Pulvirenti, *Mathematical Theory of Incompressible Nonviscous Fluids* (Springer, Berlin, 1993), Vol. 96.
[64] R. Narasimha, in *Whither Turbulence? Turbulence at the Crossroads* (Springer, Berlin, 1990), pp. 13–48.
[65] W. George and L. Davidson, AIAA J. **42**, 438 (2004).
[66] E. Balaras, U. Piomelli, and J. M. Wallace, J. Fluid Mech. **446**, 1 (2001).
[67] C. Ho and P. Huerre, Annu. Rev. Fluid Mech. **16**, 365 (1984).
[68] C. Ho and L. Huang, J. Fluid Mech **119**, 443 (1982).
[69] H. Husain and F. Hussain, J. Fluid Mech. **304**, 343 (1995).
[70] M. Gaster, E. Kit, and I. Wygnanski, J. Fluid Mech. **150**, 23 (1985).
[71] Y. Naka, K. Tsuboi, Y. Kametani, K. Fukagata, and S. Obi, J. Fluid Sci. Technol. **5**, 156 (2010).
[72] P. Chavanis, J. Sommeria, and R. Robert, Astrophys. J. **471**, 385 (1996).
[73] F. Clauser, Adv. Appl. Mech. **4**, 1 (1956).
[74] G. Corcos and F. Sherman, J. Fluid Mech. **139**, 29 (1984).
[75] G. Corcos and S. Lin, J. Fluid Mech. **139**, 67 (1984).
[76] H. Oguchi and O. Inoue, J. Fluid Mech. **142**, 217 (1984).
[77] J. Bell and R. Mehta, AIAA J. **28**, 2034 (1990).
[78] M. Slessor, C. Bond, and P. Dimotakis, J. Fluid Mech. **376**, 115 (1998).
[79] S. Kleis and A. Hussain, Bull. Am. Phys. Soc. **24**, 1132 (1979).